

DLR-IB-FA-BS-2019-18

Development of Stiffened Self-Deploying Membranes for CubeSat Applications

Masterarbeit

Jannic Völker



DLR

**Deutsches Zentrum
für Luft- und Raumfahrt**



Institut für Faserverbundleichtbau und Adaptronik

DLR-IB-FA-BS-2019-18

Development of Stiffened Self-Deploying Membranes for CubeSat Applications

Zugänglichkeit:


Stufe 2 DLR intern zugänglich: analog „allgemein zugänglich“, allerdings ist dieser in ELIB nur für intern zugänglich abzulegen.

Braunschweig, Juni, 2018

Der Bericht umfasst: 97 Seiten


Abteilungsleiter: Prof. Dr.-Ing. Christian Hühne


Autoren: Jannic Völker


Autor 2 / Betreuer:
Dipl.-Ing. Martin Eckhard Zander



DLR

Deutsches Zentrum
für Luft- und Raumfahrt



Chair of Astronautics
Prof. Prof. h.c. Dr. Dr. h.c.
Ulrich Walter



Technical University of Munich

Master's Thesis
**Development of Stiffened Self-Deploying Membranes for
CubeSat Applications**

RT-MA 2018/06

Author:

Jannic Voelker

Supervisor:

Martin E. Zander
Institute of Composite Structures and Adaptive Systems
German Aerospace Center

Florian Schummer
Chair of Astronautics
Technical University of Munich

Abstract

The German Aerospace Centre (DLR) and the National Aeronautics and Space Administration (NASA) started the Joint Deployable Space Structures project in 2016 to develop deployable structural systems for small satellites. This project focuses among others on boom and membrane deployment in the range of 5 to 20 meters boom length. This thesis is placed within a sub-project, which focuses on smaller membranes (1 m^2) for CubeSat applications. Since the boom-deployment technology encounters down-scaling problems at these sizes, a new deployment and stiffening method was developed in this thesis.

Interesting applications of membranes are solar sails, drag sails, sunshields, or as base for photovoltaic arrays. Exemplary missions and projects were studied and gave the foundation to generate applicable partial solutions.

Every possible partial solution for the deployment method, stiffening structure, distribution of stiffening structure and packaging was listed in a morphological box. These partial solutions were combined to form concepts. The result of the concept evaluation is that 3D printing of rods on the membrane is the most promising method. The rods form a specific pattern and need a hinge at the membrane folding lines, to avoid permanent deformation. These specific elastic hinges were identified as a critical component for many concepts and were therefore investigated in detail. They are 3D printed and store the deployment energy in deformation. The challenges of the concept and the hinges are the stiffness, providing a sufficient force for self-deployment and that the deformation has to stay in the elastic region to avoid permanent deformation, which would lead to an incomplete reopening.

Computer Aided Design (CAD) models of different hinge designs were constructed, printed and tested with different printers and materials. Fused Deposition Modeling (FDM) with two different materials and a layer resolution below 0.1 mm was identified as the most promising 3D printing method. The hinge design with the best reopening-angle (170°) in the tests, the Torsion-Hinge, was selected for a Finite Element Analysis (FEA).

Thereby, several improved Torsion-Hinge geometries, as well as the new 2TR-Hinge design, were identified, printed, tested and had reopening-angles of 175° and 180° . This proves the applicability of a small 3D printed elastic hinge, and paves the way for the superordinate development of the whole concept.

Contents

1	INTRODUCTION	1
1.1	DLR-NASA Joint Deployable Space Structures	1
1.2	Objective	2
1.2.1	Requirement Specification	2
1.2.2	Procedure	4
2	STATE OF THE ART	5
2.1	Photovoltaic Solar Cells	5
2.2	Deployable Solar Arrays	5
2.3	Solar Sail	8
2.4	Drag Sail	11
2.5	Sunshields	11
3	CONCEPT DETERMINATION	12
3.1	Partial Solutions	12
3.1.1	Examples in Nature	12
3.1.2	Deployment Method	18
3.1.3	Stiffening	20
3.1.4	Packaging	21
3.1.5	Membranes	23
3.1.6	Rip-Stop	24
3.2	Morphological Box	24
3.3	Combination of Concepts	26
3.4	Evaluation	39
4	ELASTIC HINGE - DESIGN AND TEST	44
4.1	Designs	44
4.1.1	Reducing the Bending Radii Difference by Design Variations	45
4.1.2	Changing from Bending to Torsion	47
4.1.3	Multiple Material Designs	48
4.2	3D Printer and Materials	49
4.2.1	Precision	51
4.2.2	Method	51
4.2.3	Material Properties	51
4.3	Tests	54
4.3.1	Form 2	55
4.3.2	Mark Two	56
4.3.3	Objet260 Connex3	57
4.4	Comparison and Selection	62
5	FINITE ELEMENT ANALYSIS	64
5.1	Model	64
5.1.1	Input	65
5.1.2	Output	65

5.1.3	Variations	66
5.2	Analysis Results	67
5.2.1	Durable	67
5.2.2	Nylon	69
5.2.3	2TR-Hinge	70
5.3	Test Results and Comparison with FEA	73
5.3.1	Durable	73
5.3.2	Nylon	74
5.3.3	2TR-Hinge	75
5.4	Conclusion	75
6	SUMMARY AND OUTLOOK	77
6.1	Summary	77
6.2	Validation Test Preparations	77
6.3	Outlook	79
	BIBLIOGRAPHY	80
A	APPENDIX	86
A.1	Torsion Hinge Mesh	86
A.2	Hinge Parameters	86
A.3	Folded Bowl Hinge	88
A.4	Folded O-Hinge	89

List of Figures

Fig. 2–1:	Dove satellite with deployed solar arrays	6
Fig. 2–2:	ISS solar arrays Z-folded	6
Fig. 2–3:	Flexible solar array on the Hubble Space Telescope	7
Fig. 2–4:	Deployment sequence of MegaFlex	8
Fig. 2–5:	Artist’s illustration of NASA’s NanoSail-D	9
Fig. 2–6:	Deploying boom	9
Fig. 2–7:	Gossamer-1 membrane stowage concept	10
Fig. 2–8:	Gossamer-1 deployment sequence	10
Fig. 3–1:	Schematic view of the Earwig hind wing	13
Fig. 3–2:	Broadened vein patch of the Earwig hind wing	13
Fig. 3–3:	Dragonfly wing	14
Fig. 3–4:	A stretched bat wing	15
Fig. 3–5:	Five kind of venation pattern	16
Fig. 3–6:	Leaves of a Jackfruit	16
Fig. 3–7:	Model of unfolding Hornbeam and Beech leaves	17
Fig. 3–8:	Tape Spring	18
Fig. 3–9:	Miura-Ori folding process	22
Fig. 3–10:	Wrapping a membrane around a hub	23
Fig. 3–11:	Concept: EAP Bat	28
Fig. 3–12:	Concept: Taut SMA	29
Fig. 3–13:	Concept: Cable Repulsion	30
Fig. 3–14:	Concept: Rigidized Web	31
Fig. 3–15:	Concept: Tensed around a Hub	32
Fig. 3–16:	Concept: Flower	33
Fig. 3–17:	Concept: Beetle	34
Fig. 3–18:	Concept: Leaf	35
Fig. 3–19:	Concept: Inflated Leaf	36
Fig. 3–20:	Concept: Rectangles	37
Fig. 3–21:	Concept: Double Folded Fan	38
Fig. 4–1:	Design: Bent Rod	44
Fig. 4–2:	Design: Wide and Flat-Hinge	45
Fig. 4–3:	Design: Bowl Hinge	46
Fig. 4–4:	Design: O-Hinge	46
Fig. 4–5:	Design: Torsion-Hinges	47
Fig. 4–6:	Design: Oval-Hinge	48
Fig. 4–7:	Design: O2-Hinge	48
Fig. 4–8:	Design: Filled-O-Hinge	49
Fig. 4–9:	Test Execution Draft	54
Fig. 4–10:	Printed Hinges, Durable	55
Fig. 4–11:	Printed Hinges, Nylon	56
Fig. 4–12:	Printed Hinges, Objet260	57
Fig. 4–13:	Design: Parabola-Hinge	58

Fig. 4–14:	Design: O4-Hinge	59
Fig. 4–15:	Design: BigHole-Hinge	61
Fig. 5–1:	Parameters of the Torsion-Hinge Model	64
Fig. 5–2:	B2_w47 Durable	68
Fig. 5–3:	B2_w45 Nylon	70
Fig. 5–4:	CAD Image of a 2TR-Hinge	71
Fig. 5–5:	2TR B2_w45 Nylon	72
Fig. 6–1:	Counter-Weight Balanced Column Bending Test Fixture	78
Fig. A.1:	Mesh of the B2_w45 Nylon Hinge	86
Fig. A.2:	Folding and Reopening of the Bowl Hinge	88
Fig. A.3:	Folding of the O-Hinge	89

List of Tables

Tab. 3–1:	Morphological Box	25
Tab. 3–2:	Concept Combination Matrix	27
Tab. 3–3:	Evaluation Matrix	40
Tab. 4–1:	3D Printer Characteristics and Materials	50
Tab. 4–2:	Material Properties 1	52
Tab. 4–3:	Material Properties 2	53
Tab. 4–4:	Test Results Parabola-Hinge	58
Tab. 4–5:	Test Results O2-Hinge	59
Tab. 4–6:	Test Results Oval-Hinge	60
Tab. 4–7:	Test Results BigHole-Hinge	61
Tab. 4–8:	Test Results short Torsion-Hinge	61
Tab. 4–9:	Test Results long Torsion-Hinge	62
Tab. 5–1:	Input Parameters of the B2_w-47 Durable Torsion-Hinge	68
Tab. 5–2:	Input Parameters of the B2_w-45 Nylon Torsion-Hinge	69
Tab. 5–3:	Input Parameters of the 2TR B2_w-45 Nylon Hinge	72
Tab. 5–4:	Test and Analysis Results Durable Hinges	73
Tab. 5–5:	Test and Analysis Results Nylon Hinges	74
Tab. 5–6:	Test and Analysis Results Nylon 2TR-Hinges	75
Tab. A.1:	Parameters and Analysis Results of Torsion-Hinges	87

Acronyms

ABS	Acrylnitril-Butadien-Styrol
ALM	Additive Layer Manufacturing
APDL	Ansys Parametric Design Language
CAD	Computer Aided Design
CG	Center of Gravity
DLR	German Aerospace Centre
EAP	Electroactive Polymers
ESA	European Space Agency
FDM	Fused Deposition Modeling
FEA	Finite Element Analysis
FEM	Finite Element Method
IFA	Institute of Composite Structures and Adaptive Systems
IKAROS	Interplanetary Kite-craft Accelerated by Radiation Of the Sun
ISS	International Space Station
JAXA	Japan Aerospace Exploration Agency
JPL	Jet Propulsion Laboratory
JWST	James Webb Space Telescope
MIT	Massachusetts Institute of Technology
MJM	MultiJet Modeling
NASA	National Aeronautics and Space Administration
PET	Polyethylene Terephthalate
PETG	Polyethylenterephthalat + Glykol
PLA	Polylactide
SLA	Stereolithography
SMA	Shape Memory Alloy
TRL	Technology Readiness Level

1 Introduction

Reducing the mass of a spacecraft is important for lowering the price of launching and decreasing the fuel consumption. Therefore a lightweight design is important for every part of a spacecraft. While the mass and size of spacecraft (components and subsystems) are generally decreasing [1], components that collect or reflect photons and electromagnetic radiation, can not be decreased in size. For example, the area of solar arrays or the size of an antenna is not related to the overall spacecraft size, but to the energy generation, consumption and the position of the spacecraft. To significantly reduce the volume at launch of these subsystems, they have to be expanded in orbit.

This does not only apply for small spacecraft. The James Webb Space Telescope (JWST), for example, has a mass of about 6200¹ kg and its size (21 m * 14 m) is restricted to the payload volume of the launcher (4.6 m diameter, 16.2 m length). Therefore, it uses a series of deployments of the segmented mirrors, solar arrays, antenna, and multiple layers of a sun-shield membrane. [2]

A spanned membrane has further interesting areas of application. Reflective membranes can use the radiation pressure of the sun to accelerate a spacecraft (see Chapter 2.3), drag sails can increase the atmospheric drag and therefore reduce the time in orbit after retirement (see Chapter 2.4), or the membrane can be used as base for solar cells or antennas.

1.1 DLR-NASA Joint Deployable Space Structures

In the 1990s, research in this field started with breadboard tests of a 20 m * 20 m solar sail, in a joint DLR, NASA, Jet Propulsion Laboratory (JPL) and European Space Agency (ESA) project. This was followed by DLR's Odissee and Geosail projects, which planned to use a solar sail for a scientific payload. However, these projects have been identified as too complex and the project Gossamer was started in 2009. The objective was to develop a scalable solar sail for technology demonstration, starting with a 5 m * 5 m sail on Gossamer-1, 25 m * 25 m on Gossamer-2 and 50 m * 50 m on Gossamer-3. [3]

The funding for the Gossamer project was cut in 2015 [4]. In the same field, but unrelated to these projects, DLR² and NASA³ began the Joint Deployable Space Structures project for small satellites in 2016.

Scaling down existing large boom designs leads to manufacturing issues due to limited packaging volume. Therefore, boom and membrane deployment concepts for small satellite applications, such as solar arrays, solar sails, drag sails and instrument booms, shall be developed in this project. The targeted size for the booms is 5 to 20 m and

¹ Including fuel and launch vehicle adaptor

² Institute of Composite Structures and Adaptive Systems, Braunschweig, Germany
Project Management: Institute of Space Systems, Bremen, Germany

³ Langley Research Center, Virginia, USA

the design shall be scalable within this range. The project shall finish after about three years with testing the concepts on the ground and on parabolic flights, in order to achieve a Technology Readiness Level (TRL) of 6. [1]

The key challenges are: [1]

- Thermal stability and stiffness of the boom
- Tolerance to boom manufacturing imperfections
- A deployment mechanism that is simple, testable on the ground and reliable, even after being stowed for many years. (A drag sail, for example, is only needed after an operational lifetime of up to 10-15 years.)

1.2 Objective

This thesis is placed within a sub-project of the project described above. The intention is to develop a smaller membrane, suitable for CubeSat¹ applications (not exclusively). The application of the membrane is not yet specified.

The boom-deployment technology from the project described above encounters down-scaling problems at these sizes, because of the coil radius and basic mass for the deployment mechanism. So, without booms, a new deployment method and a stiffening structure for the membrane are needed.

This sub-project has these two main objectives:

- Developing a stiffening structure for a membrane. The structure shall be lightweight and integrated into or distributed onto the membrane, so that the membrane can be folded or rolled up inside a CubeSat.
- Developing a deployment method requiring low volume and mass. Investigating the possibility of self-deployment through stored intrinsic energy.

1.2.1 Requirement Specification

Sources for these more detailed requirements are intern presentations about the project by DLR and NASA and my supervisor Martin E. Zander. The Requirements are separated into a Demonstration Mission (proof of concept on parabolic flight tests) and the final Satellite Mission.

Because of the early phase of the study, few numerical values are given for the requirements. These values will result from analysis of the concepts and then will be used to compare the concepts.

¹ A CubeSat is a small satellite with standardized dimensions of 10 cm * 10 cm * 10 cm and a maximum of 1.33 kg per unit (1U). So a 3U CubeSat has the dimensions 30 cm * 10 cm * 10 cm and can have a mass of 4 kg.

1.2.1.1 Satellite Mission

The requirements for the final satellite mission, the objective of this sub-project:

General

- G1 The objective is to deploy a membrane in space, which shall be applicable for 3 to 30 kg satellites.
- G2 The concept shall occupy a small volume when stored.
- G3 After deployment the membrane shall have a plain area of 4 m²
- G4 The concept shall be lightweight.
- G5 The concept should be low cost.
- G6 The materials used shall withstand the space environment.

Deployment

- D1 The deployment shall change the membrane from its packed state into a plain area.
- D2 The deployment complexity shall be reduced (compared to the typical sail architecture described in Chapter 2.3).
 - D2.1 The deployment may be uncontrolled.
 - D2.2 The deployment may be not retractable.

Structure

- S1 The structure shall provide a flat membrane.
- S2 The structure shall provide areal stiffness.
- S3 The structure shall withstand the loads induced by solar cells or solar pressure or aerodynamical pressure.
- S4 The structure shall be distributed and integrated into the membrane.

Rip-Stop

- R1 Rips shall be stopped from growing larger than 10 cm.
 - R1.1 A rip-stop pattern should be distributed over the membrane.
 - R1.2 The structure should be a part of the rip-stop.

1.2.1.2 Demonstration Mission

For now, the development shall conclude with two concept demonstrators, being deployed on parabolic flights. The requirement changes and additions for this demonstration mission are:

General

- G1 The objective is to develop a demonstrator, which shall be suitable for 3U and 6U CubeSats.
- G1.1 The stored base area dimensions shall not exceed 28.7 cm and 18.3 cm for 6U or 28.7 cm and 8.3 cm for 3U.¹ The third dimension shall be small.
- G3 After deployment of the demonstrator, the membrane shall have a plain area of 1 m².
- G6 The materials used for the demonstrator may not be space qualified.

Deployment

- D3 The deployment shall be testable in a 1g environment.
- D4 The deployment shall be tested on a parabolic flight. Therefore, it should deploy in under 18 seconds, which is the time of one 0g phase during the parabolic flight.

1.2.2 Procedure

The state of the art of every sub-function of every possible solution is compiled and listed in a morphological box, together with further possibilities. Partial-solutions from this morphological box are combined to concepts and in the next step, these concepts are evaluated and the best are selected for further analysis.

A CAD model is constructed of the selected concept, to allow a Finite Element Method (FEM) analysis about the behavior and stability of the design. This is done in an iterative manner, studying different materials and dimensions. The outcomes are evaluated and the best concept is selected for experimental validation.

Since this thesis is conducted at an early point in the project, a physical implementation of the concept is not part of the thesis.

¹ Derived from [5]: Maximum dimension of each 6U or 3U CubeSat axis, minus 8.5 mm for each rail or 6.5 mm for each standoff.

2 State of the Art

Since the initial idea was using the membrane as base for solar cells, the state of the art technology for solar cells is examined first, followed by applications of deployable membranes.

2.1 Photovoltaic Solar Cells

Photovoltaic solar cells fixed on rigid panels are used on most spacecraft operating in the inner Solar System. Rigid cells and panels, however, are not considered in this thesis, because the objective is to study membranes and the possibility of using these as a base for flexible and foldable solar cells.

Solar cells generally do not have to be thick. The active semiconductor material absorbs most photons within the first $10\ \mu\text{m}$. The thickness is mainly formed by the additional layers of adhesive, cover glass, antireflective coating and a substrate [6]. But these can be reduced drastically.

For example, in 2011, the Massachusetts Institute of Technology (MIT) developed a process of printing solar cells onto a substrate (e.g. paper or Polyethylene Terephthalate (PET)), which then is foldable [7]. In 2016 another ultrathin and flexible solar cell prototype has been developed at MIT. These cells are so light that even though the efficiency is low, they demonstrated a great power-to-weight ratio of $6\ \text{kW/kg}$ [8]. Further examples, mentioned in Chapter 2.2, are blanket solar arrays of the Hubble Space Telescope and the ROSA Experiment, or thin film solar cells used on the IKAROS sail. The IKAROS solar cells produce up to $500\ \text{W}$ on $20\ \text{m}^2$ with a thickness (including membrane) of 170 to $200\ \mu\text{m}$ [4].

The most important characteristics for solar panels used in space are the power-to-mass-ratio (W/kg) and its Volume during launch (W/m^3 folded). This means that even though the efficiency (W/m^2) of flexible solar cells is lower (but increasing) [9], the more important characteristics of power-to-mass-ratio and volume during launch can be better than for rigid cells. A limiting effect is the stability of those membranes and the mass increase due to deployment mechanism and stiffening structure. This is examined in this thesis.

2.2 Deployable Solar Arrays

Many modern spacecrafts use deployable solar arrays for energy generation. Typically the solar cells are fixed on rigid body elements, which are connected with hinges. The elements are folded during launch and deployed in orbit.

CubeSats typically use body mounted solar cells because of their small size. However, some CubeSats (like MOVE-II [10]) also deploy their solar arrays, which are the size of the CubeSats surface. To increase the power generation further, the HaWK solar

arrays of the company MMA Design LLC [11] or the Dove CubeSats deploy a multiple of their side surfaces. These are competitors, regarding a Solar Array application of the membrane.

Dove Satellites

Dove is the name of 3U CubeSats of the company Planet Labs, used for Earth observation [12]. It can be seen in Fig. 2–1 after deployment of the solar arrays. There are three panels on both sides of the CubeSat. This adds up to an area of approximately $7 \cdot 10 \text{ cm} \cdot 30 \text{ cm} = 0.21 \text{ m}^2$.



Fig. 2–1: Dove satellite with deployed solar arrays [12]

International Space Station (ISS)

A variation of this unfolding technique, using solar cells on a thin flexible body, has been used for the ISS. The so-called tensioned blanket solar array was Z-folded (explanation in Chapter 3.1.4) during launch and was pulled apart by a truss, unfolding them into a planar surface of 150 m^2 per wing. The folding lines are reinforced by hinge bands (the white parts in Fig. 2–2) and located between the solar cells, which leaves the solar cells rigid. [4]

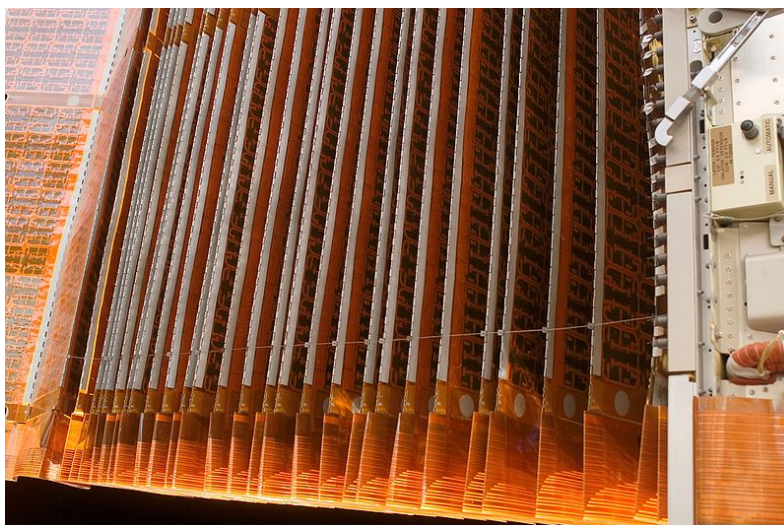


Fig. 2–2: ISS solar arrays Z-folded [13]

Hubble Space Telescope

Flexible solar cells have been used on the Hubble Space Telescope, fixed on a tensioned blanket solar array (see Fig. 2–3). The deployment method was different for the ISS. The blanket was unrolled from a cylinder, being pulled by two booms made out of strips of steel in a circular cross section. Before the deployment with a motor, the strips were flat and rolled up. [14]

Soon after deployment, vibrational disturbances were observed, which were thermally induced during orbital day-night crossings.

The control system was updated to attenuate the disturbances and later, new solar arrays, which were mechanically and thermally redesigned, were installed during the first servicing mission. [14]

This shows a problem with thin structures and membranes. They have low natural frequencies and a low damping rate. Furthermore, the objective is often to point at the sun, which leads to large thermal loads and strict orientation requirements despite the disturbances. Moreover, this is hardly testable on the ground.



Fig. 2–3: Flexible solar array on the Hubble Space Telescope [4]

ROSA

The “Roll-Out Solar Array” (ROSA) Experiment used a similar technique to that of Hubble and has been tested on board of the ISS in 2017 [15].

MegaFlex

UltraFlex and MegaFlex are products of the company Orbital ATK. It is an accordion fanfold flexible blanket solar array, deployed as seen in Fig. 2–4. UltraFlex has been used on NASA's Phoenix Lander and Cygnus ISS resupply missions. MegaFlex has been developed for NASA's Solar Electric Propulsion systems and is based on the UltraFlex design, but thinner, due to the way it is folded. [16, 17]

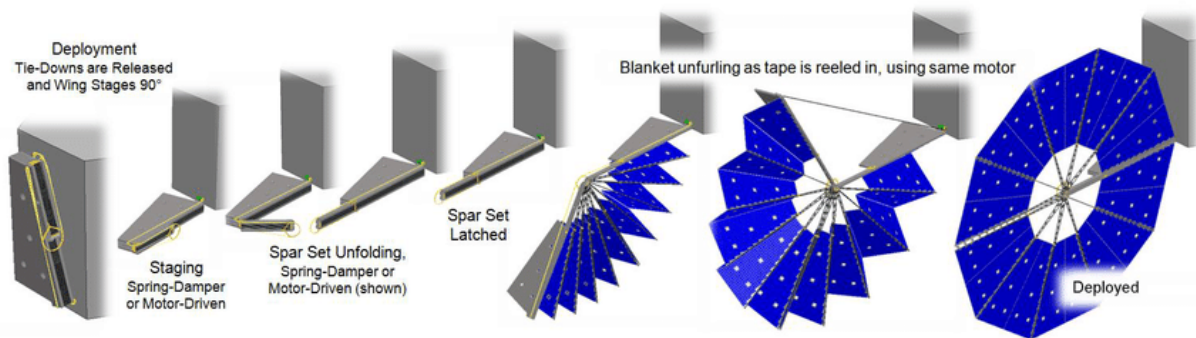


Fig. 2–4: Deployment sequence of MegaFlex [4]

2.3 Solar Sail

Solar sailing is a concept for propulsion in interplanetary space, using the radiation pressure of the sun. A large reflective membrane is deployed from a lightweight spacecraft, to reflect photons in a specific direction and thereby gains an impulse in the opposite direction. The exerting force is smaller by multiple orders of magnitude than in chemical propulsion, but acts constantly and it does not require fuel. Therefore, the spacecraft has to be very light and the area of the sail large. Such a sail has to be folded to fit into a rocket. [18]

A few examples are given here, even though the design of these sails differentiate from the design-task at hand for this thesis:

IKAROS

Interplanetary Kite-craft Accelerated by Radiation Of the Sun (IKAROS) was the first spacecraft to successfully use solar sailing as propulsion method. Launched in 2010 by Japan Aerospace Exploration Agency (JAXA) onto a Venus transfer orbit, it reached Venus six months later, having accelerated by 100 m/s through radiation pressure. The IKAROS spacecraft was spinning and used centrifugal forces for deployment and stabilisation, with tip-masses in the corners of its 14 m * 14 m square sail. In addition to solar sailing, the deployed membranes were used as a base for thin-film solar cells. [18]

Typical Sail Architecture

The typical architecture for sails (see Fig. 2–5) consists of four booms deploying from the spacecraft in a X-configuration.



Fig. 2–5: Artist's illustration of NASA's NanoSail-D [19]

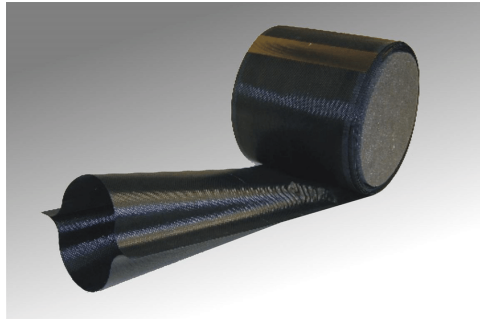


Fig. 2–6: Deploying boom [4]

The boom is usually flat and rolled-up during launch and is deployed in orbit. A motor or tension within the rolled-up state unrolls the boom, which changes its cross section to a stiffer “double-omega” form. Both states can be seen in Fig. 2–6. For details on boom design see [1] or [20].

At the same time or after boom deployment, four rectangular membranes connected to the tip of the boom, are pulled out of the spacecraft. These membranes have been folded and/or rolled up before launch. This can be seen in Fig. 2–7 for the Gossamer-1 membrane, which includes experimental thin-film solar cell modules adhered to the membrane. The main design driver for this pattern are volume efficient folding and a tensioned membrane during the whole deployment process. Otherwise, the membrane can become entangled with other membranes or the boom and consequently

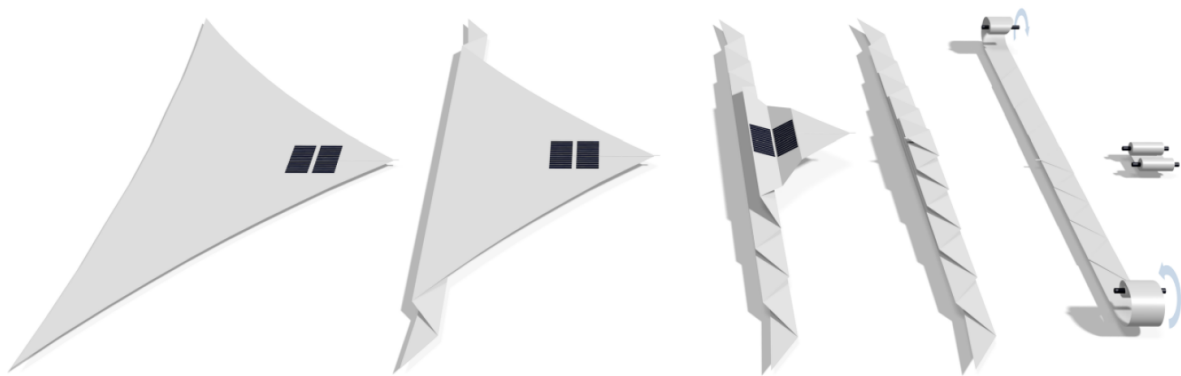


Fig. 2-7: Gossamer-1 membrane stowage concept [4]

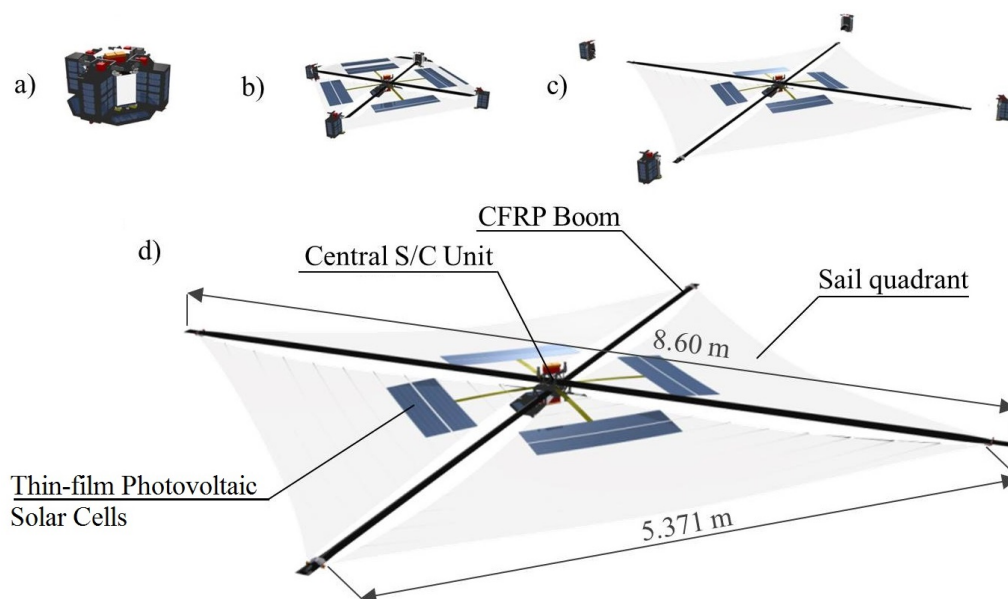


Fig. 2-8: Gossamer-1 deployment sequence. Edited from [21]

tear when tensioned again. In addition to this, air inclusions during folding on the ground are a problem. When the membrane reaches orbit the air expands and can tear the membrane. [4]

The deployment sequence is shown in Fig. 2-8. The booms and sails are stored within four containers in a). In b), the deployment sequence has been started and finished with the jettisoning of the containers in c). d) shows the deployed architecture of the Gossamer-1 concept.

This architecture has been studied at the DLR since the 90's, in the subsequent Gossamer project and the current DLR-NASA Joint Deployable Project. NASA used this architecture on the NanoSail-D missions (artist's illustration in Fig. 2-5), the cancelled Sunjammer and the planned Near-Earth Asteroid Scout mission. LightSail-1 was a successful technology demonstrator mission from The Planetary Society, who are planning to launch LightSail-2 in 2018. [18]

Solar Kite

Solar Kite was a DLR concept downsizing the typical solar sail architecture into a 1U CubeSat. This would raise the natural frequencies and reduce complexity and risk. The concept was not pursued further after the first study. [22]

2.4 Drag Sail

Alike the solar sail, a drag sail is deployed from a spacecraft to increase its area. Unlike the solar sail, this is done to enhance the aerodynamic drag of a spacecraft in Earth's orbit. The objective is quick deorbiting of the spacecraft after it has finished its operation, to decrease the amount of orbital debris in Earth's orbit. This task does not start until the primary mission is completed, which can take up to 10-15 years. The very long stowed lifetime results in difficulties for material selection, mechanism design and tests. [1]

The architecture of a drag sail is similar to the typical architecture of a solar sail, with changes regarding the stability and the membrane properties.

DeorbitSail

DeorbitSail was a joint project between Surrey Space Center and the DLR. The DLR developed booms and its deployment system for a 3U CubeSat mission, launched in 2015. The objective was to deploy the 4 m * 4 m drag sail for a technology demonstration, but the deployment could not take place due to software and electronic issues of the spacecraft. [1]

2.5 Sunshields

To increase the thermal stability, some spacecraft have to be shielded from the Sun's radiation. This is especially important for astronomy spacecraft, like ESA's space observatory Gaia or the JWST.

The infrared-optimized JWST has to decrease the background noise level of every heat source. Therefore, five layers of a membrane are deployed in space, to shield the telescope from the sun and its own warm spacecraft components. Additionally, this reduces thermally induced distortions of its optical instruments. [6]

More information and a video of the deployment can be found at [23].

3 Concept Determination

In the first section, ideas and inspirations for possible partial solutions are collected, explained and subsequently listed in a Morphological Box. The elements of the box are then combined to generate concepts, which are explained and evaluated.

3.1 Partial Solutions

In this section, every method or technique, which can be a partial solution regarding each category, is explained. These categories are the deployment method, the packaging, the stiffening structure and its distribution, which is inspired by nature. Further categories are the membrane material and the method to stop rip propagation.

3.1.1 Examples in Nature

As an inspiration for folding, deployment and the distribution of stiffeners within the membrane, nature shall be considered. In the process of evolution, nature has formed optimal solutions for specific tasks, some of which can be adapted. They are listed here.

Membranes, which have a lightweight stiffening pattern can be found in insect wings. These wings additionally often fold up and have a self-deployment mechanism. Other examples are bat wings, spider webs and leaves.

Earwig

The hind wing of an earwig bug (Dermapteran) is shown in Fig. 3–1. The unfolded wing has a ten times greater area than when it is folded. The veins, which are the stiffening structure, are depicted as thick black lines. They radiate from the center of the wing, rather than from its base. Another interesting stiffening mechanism is that the membrane is not perfectly flat. At the mid-wing mechanism, the sum of folding-angles is less than 360° , which forms the stopping point of the wing deployment [24].

The lines of folding are the thin dashed lines and the direction is indicated by +/up or -/down. The wing is folded four times in one combined movement: fan-wise radially, twice transversely (ring fold and transverse fold) and longitudinally. The folding is done through elastic energy, stored by resilin in the broadened vein patches and along the folds. The unfolding is done by a different body part, the cerci (extension of the abdomen). This is reverse to the intended spacecraft application, where the unfolding shall be done by intrinsic energy. [25]

Resilin is a rubber like protein, e.g. used in the jumping mechanism of flea or grasshopper legs. The resilin distribution of one broadened vein patch and folding line can be seen in Fig. 3–2 (of which the image section is marked with a red “P” in Fig. 3–1). The black parts on the left and right side are a normal vein, which are connected by a bigger light blue spot in the middle, which is the resilin (The picture is made with blue

autofluorescence light to show the presence of resilin). The folding line (the light blue line on the top of the picture) is made of resilin, too.

The broadened vein patches along the ring fold store elastic energy like a spring. Furthermore, by splitting up the vein, its diameter is reduced and the bending radius of the folding can be smaller. This makes the broadened vein patch, subsequently called “O-Hinge”, an interesting deployment mechanism that has been tested in [6].

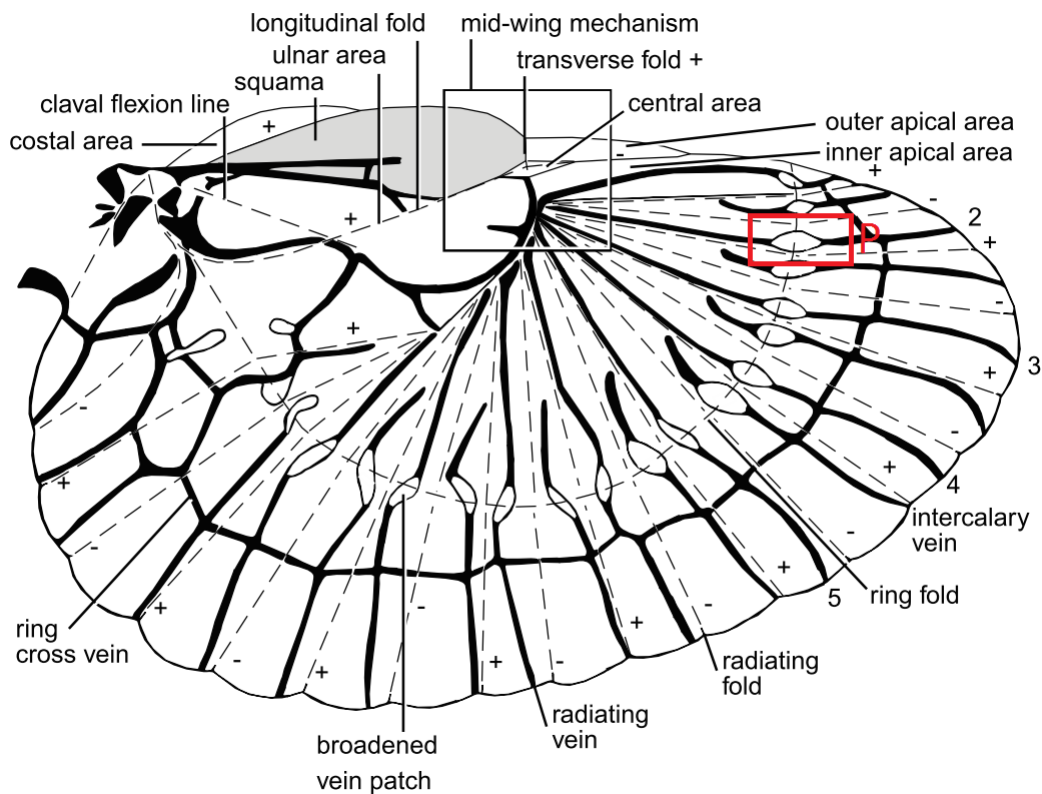


Fig. 3–1: Schematic view of the Earwig hind wing [25]

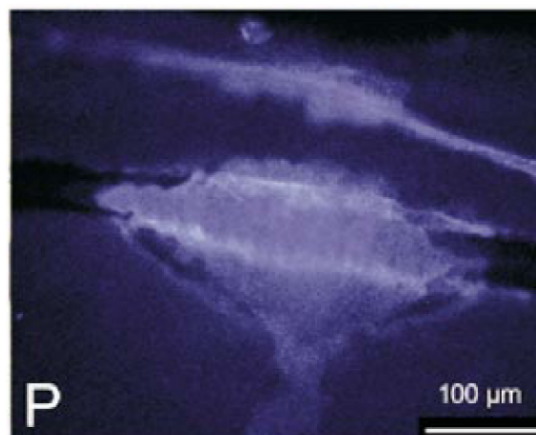


Fig. 3–2: Broadened vein patch of the Earwig hind wing [25]

Dragonfly

Resilin is found in the Dragonfly (Odonata), too, but only in the joint of the wing and body. Its wings are stored on top of its body and not folded. Only after hatching, the wings irreversibly inflate to their normal size and then harden in the sun. [26]

The most interesting aspect of the Dragonfly wing is the vein pattern depicted in Fig. 3–3. This pattern is not only used for stiffening the membrane, but also to stop damage from propagating. The leading edge consist mostly of rectangular angles, because here the veins are mainly spacers for the three-dimensional aerodynamic profile of the wing. Whereas the rest of the wing is mostly formed of hexagons. In a hexagon, the angle between two veins is 120° , which is the best angle to evenly distribute a force within a plain network. [26]

Since every species has a different vein pattern, there are numerous examples (like Beetles, Grasshoppers or Cockroaches). In [27], 16 different insect wings are related to a phylogenetic tree.

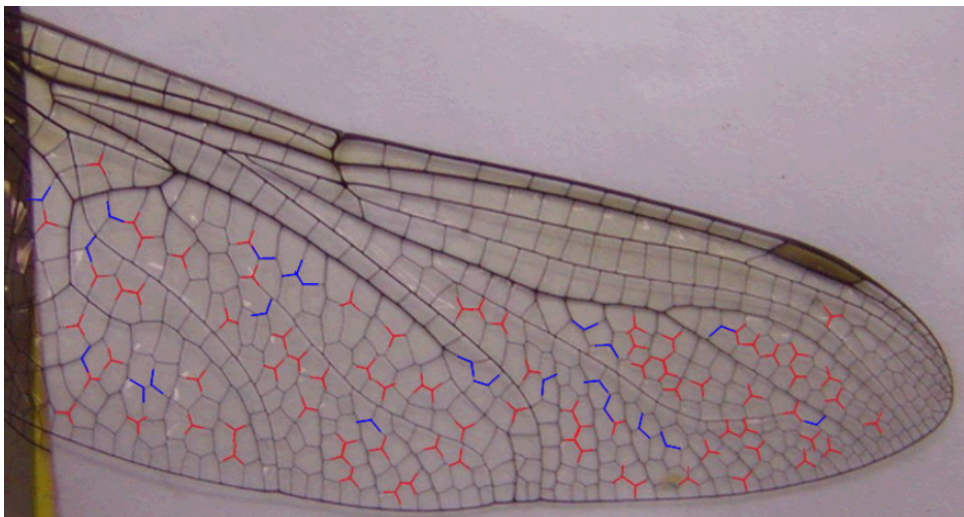


Fig. 3–3: Dragonfly Aeshna Mixta wing, 120° angles marked red and blue [26]

Bat

Bat wings use a different principle, where the membrane is elastic and tensioned between the bones. The deployment mechanism are its muscles. The distribution of bones (see Fig. 3–4), the vein network, wing folding and deployment are interesting and are added to the morphological box. When folding, the fingers go towards the forearm, the elbow goes down and the forearm retracts closer to the body.

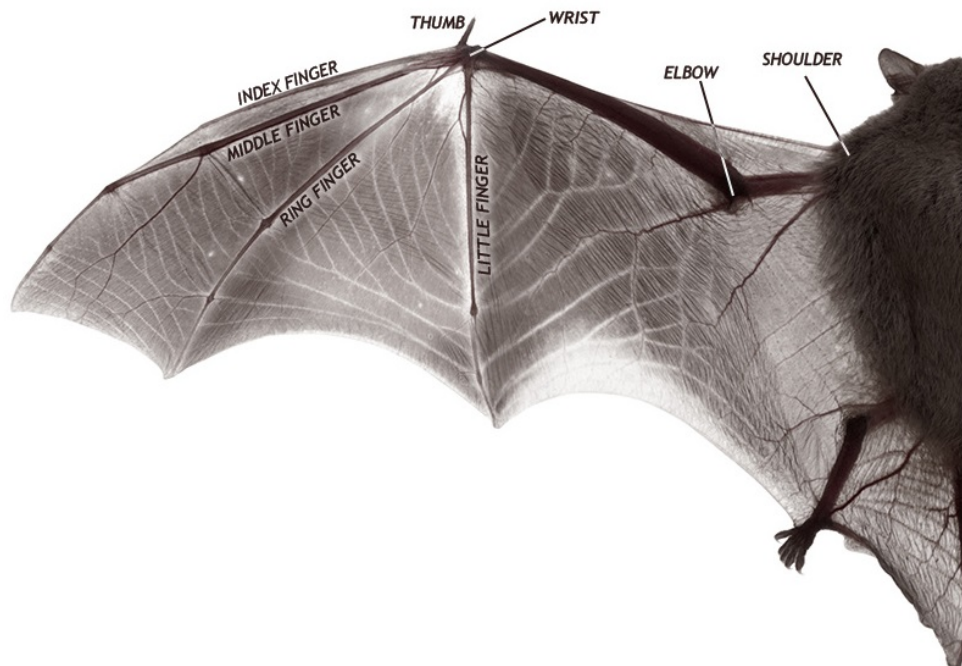


Fig. 3–4: A stretched bat wing, [28] with inverted colors

Spider Web

A spider web is a good example for the distribution of stiffeners and rip-stop, if the membrane is partly circular.

Leaf

The evolutionary driver of making leaves lightweight is not flying, as for insects, but the reduction of needed material. The leaf and its venation pattern differ from insects, as these are symmetrical and branching, instead of a cell-like structure of insect wings. The venation pattern is different for every plant and can be categorized into five basic kinds shown in Fig. 3–5. These venation patterns can be used as a example for the distribution of stiffeners on the membrane.

- Arcuate: The secondary veins are bending towards the tip. (e.g. Jackfruit, Fig. 3–6)
- Palmate: Several primary veins diverging from the center.
- Parallel: The veins are intersecting only at the tip.
- Pinnate: The secondary veins emanate straight from the primary vein.
- Reticulate: A network of veins - often combined with one of the patterns above.

VENATION

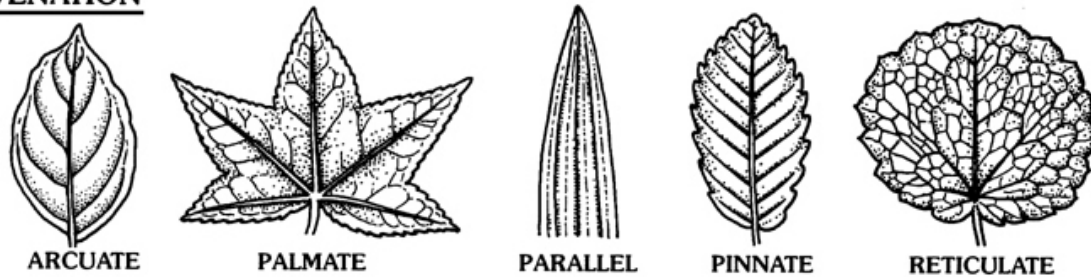


Fig. 3–5: Five kind of venation pattern [29]



Fig. 3–6: Leaves of a Jackfruit [30]

The leaves of a Jackfruit are Arcuate and Reticulate. The network of veins can be seen in Fig. 3–6 and one can see that the Arcuate structure makes the tip wider than the base of the leaf. This structure can be practical if the leaves are connected to the branch in a circular manner, because then the base of a leaf does not cover the leaf next to it.

This shows that there is an interdependency between the shapes of the leaf and the vein structure. The shapes of a leaf are not listed here because of endless possibilities, but can be seen as a possible inspiration from nature too.

Mechanisms

Some leaves roll up when a strong wind is blowing and elastically unfurl when the wind is gone. This can be seen as a self-deployment mechanism.

Most leaves are rolled or folded when inside the bud, but only few studies have been done from a mechanical point of view. The Hornbeam and Beech leaves have a simple

regular folding pattern and deployment method known as Miura-Ori, as seen in Fig. 3–7 [31]. They have a straight central vein and symmetrically arranged parallel lateral veins, generating a corrugated surface, which gives the leaf its stiffness [32]. The Miura-Ori folding pattern is special, because a movement in one plane (angle θ in the Y-plane) leads to a deployment in multiple planes (X/Y/Z-plane).

The conclusion of [31] is that the vein angles from the tip to the petiole range from 30° to 50° . Large vein angles can be folded more compactly but need more energy for unfolding, while small angles can be deployed quicker.

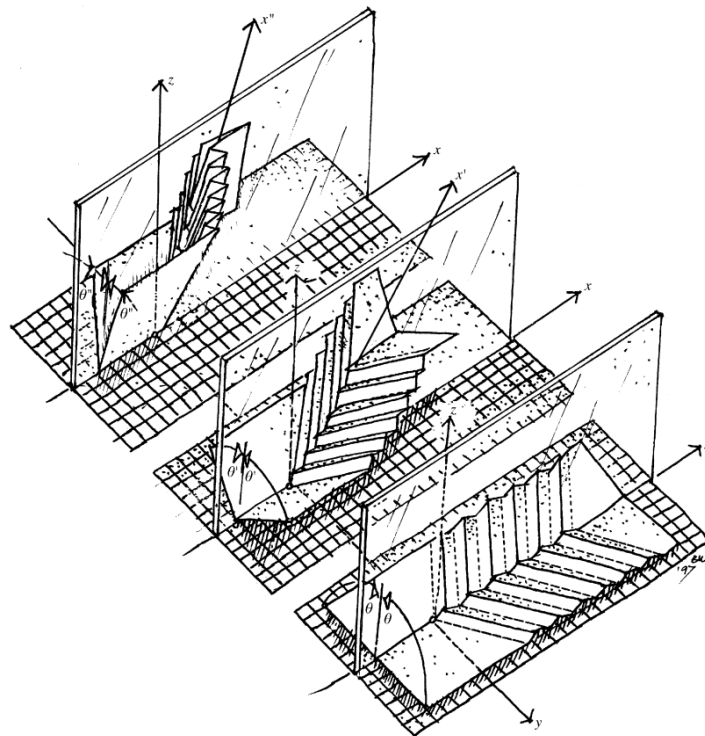


Fig. 3–7: Model of unfolding Hornbeam and Beech leaves [31]

Conclusion

For the distribution of stiffeners and a rip-stop pattern on the membrane, many examples can be considered. A spider web structure is best suited for circular membranes, while the stiffness of bat wings comes from the tensioning between its bones. The earwig wing has a great unfolded to folded area ratio, which is important for applications on CubeSats. Another interesting aspect is the foldable stiffening structure of its wings, called the O-Hinge. Insect wings have a cell-like structure, made for keeping up the wing shape, while loaded with forces during flight. Leaves, on the other hand, have a symmetrical, branching venation pattern, which allows the flow of nutrients through the leaf. This principle can be used for inflation of the membrane and the growing size of veins towards the joint can inspire the solar cells wire distribution. Leaves like the Hornbeam have a corrugated surface, which gives the leaf stiffness and a deployment method out of the bud.

3.1.2 Deployment Method

This section describes every possible method to deploy a membrane out of a CubeSat.

Motor

Using a motor is a common way of deployment, but is avoided here to save volume, mass and reduce complexity.

Tensed Structure

Using tension, often in form of a spring, is another typical way of deployment. The Earwig (Chapter 3.1.1) uses tension with its O-Hinges. One interesting example are mini rods, which are distributed over the membrane, while being foldable and tense when folded.

Boom

The boom used in the typical solar sail architecture described in Chapter 2.3 is pressed flat and rolled onto a cylinder. During deployment, it unrolls and changes its cross section to form a boom (see Fig. 2–6). For details on boom design, see [1] or [20]. A small version of this boom, applicable for CubeSats, has been tested in [22].

Tape Spring

For downscaling the boom, the design can be reduced to just an arc, which is called a “Tape Spring” (Fig. 3–8 (a)). This has been used, for example, on the Drag Sail of the TechDemoSat-1 satellite [33].

It does not have to be used as a long boom, but can also be applied as a “Tape Spring Hinge” (Fig. 3–8(b)).



Fig. 3–8: (a) Tape Spring Boom [34], (b) Tape Spring Hinge [35]

Inflation

Filling an elastic structure with a gas has been studied, tested and used in multiple areas of application. Some examples are listed here: [6, 36]

- The 30 m diameter ECHO Ballon Satellite.
- The Inflatable Antenna Experiment, flown in 1996, inflated a 14 m diameter parabolic antenna, attached to the spacecraft by 28 m long inflatable struts.
- Air bags for impact attenuation when landing Pathfinder on Mars.

- Human habitats, like the Bigelow Expandable Activity Module, currently tested on the ISS.
- Teledesic 3.6 m * 10 m solar array demonstrator.
- JPL's Advanced Radar Technology Program.
- In 2001, the Cosmos 1 spacecraft should have deployed eight solar sail segments by inflating tubes on the edges, but the rocket failed. [37]

Inflating little tubes to stretch out a membrane has been tested in [22]. A deployment was achieved, but the tests were stopped early when the material/adhesive failed. The problem is that the adhesive is loaded with peel stress, which is the worst kind of stress for adhesive bondings. Using a tube would solve this problem but increase the weight and volume.

[22] says that inflatable structure applications in space did not have a breakthrough yet, because more development, especially in the area of material science, is needed.

Shape Memory Alloy

A Shape Memory Alloy (SMA) is an alloy that can be deformed or folded and stays in that form, until it is heated and returns to its pre-deformed, original shape. A one-way SMA stays in its original shape, independent of the following temperatures. A two-way SMA can change the shape again when cooling down, so it has two original shapes depending on the temperature. [38]

A SMA can be heated by applying electrical current or by external measures. This can be useful, for example if the sun's heat is used to deploy, or problematic when a two-way SMA moves through the sun's heat and earth's shadow, which will lead to two very different temperatures.

SMA threads can spread over or within the membrane, or the whole membrane can be made out of or covered by a SMA. Thin film Nickel Titanium (NiTi) added to membranes as a deployment method has been studied in [39].

Electroactive Polymers

Electroactive Polymers (EAP) can change their size or shape in response to electrical stimulation and are also called artificial muscles. Most typical areas of application are imitation of biological characteristics and robotics. [40]

An interesting application in space, for example, is the controlling of surface shape and focal length of a thin-film mirror.

Advantages of EAP are their low density, formability, vibration damping, damage tolerance and large actuation strain. An EAP can multiply its area by up to 380%, while typical values are 10 to 100%. [40]

However, even a quadruplication of the area is not enough for the proposed applications. Furthermore, thin film solar cells would be difficult to integrate. Therefore, EAP would be used as a mechanism at specific points in the architecture, not as an overall stretching of the membrane. For example, if the membrane is merging with EAP at the

point of connection to the CubeSat, the tension in the membrane can be measured and controlled.

There are two different EAP types: Ionic and Dielectric.

Ionic EAP requires low voltage, but a permanent high electrical power to keep its position. This is problematic because after membrane deployment, no energy should be needed. Turning it around, so that the EAP is powered in the packed state, is not practical either, because CubeSats must be switched off during launch. Furthermore, ionic EAP needs to be in a wet environment, which means more layers to encapsulate the EAP and an increase in mass.

Dielectric EAPs require low electrical power, very high voltage and no power to keep its position. They do not need a wet environment, but outgassing must be considered and may cause restrictions. [40]

Since the technology itself is not mature enough, it would substantially increase the development and product complexity.

Electromagnetic Repulsion

When a current flows in alternating direction through wires laying on top of each other, an electromagnetic repulsive force is created. If the wires are distributed over the membrane in a specific way, electromagnetic repulsion deploys the folded membrane. However, the force is decreasing exponentially with the angle between the wires and will probably not be sufficient for the complete deployment by 180° . For example, a current of 2 A in two 10 cm wires creates a torque of $9 \cdot 10^{-7}$ Nm at an angle of 20° and $1 \cdot 10^{-7}$ Nm at an angle of 90° . [41]

Centrifugal Forces

For an even deployment around a rotatable axis, the centrifugal force can be used. This has been done for the IKAROS Missions to deploy a sail, as mentioned in Chapter 2.3. This is an easy technique, but it needs fuel for the initial spin and a rotating spacecraft has other disadvantages. On the other hand, not the whole spacecraft has to spin, but only the sail and attachments. [18]

3.1.3 Stiffening

Many deployment methods go hand in hand with stiffening structures, like the SMA, inflation, a tape spring or tensed mini rods. This stiffening structure has to be distributed over the membrane.

The distribution could be scattered randomly (Irregular Mesh) or with a regular pattern, like a grid (Regular Mesh), but both are inefficient [6]. For an efficient distribution of stiffeners, we have examined examples from nature in Chapter 3.1.1.

Other aspects of stiffening are:

Profile

The SMA or mini rods could have a specific profile to make them lighter, but the limiting factor will be the manufacturing technique and thickness.

Rigidizing

Some Materials can rigidize through ultraviolet radiation, evaporation, thermally or through a specific gas used in the inflation deployment method [22].

Membrane Taut Frame

A membrane is pulled taut by a frame, like the typical mast sail architecture. Other examples are a foldable frisbee, a drop flag or a pop-up tent. Booms will not be considered for Membrane Taut Frames, so that the concepts of this thesis will vary from the typical solar sail architecture.

Membrane Shape

The membrane should be flat for an efficient usage of the sun's energy. A deviation of a few degrees, however, barely changes its effectiveness. Therefore a wave form or a bi-stable unfolding inspired by the earwig (see Chapter 3.1.1), can increase the bending stiffness with small influence on the effectiveness.

Cable Harness

If solar cells are placed on the membrane, these cells will need a cable harness, which could be used as a stiffening structure to reduce mass and the number of components. However, this is very complex and the folding of electrical wires is usually avoided because they are fracturable and likely not as elastic as needed for the stiffening structure.

3.1.4 Packaging

To store the membrane inside the CubeSat it has to be packed. It can be randomly crumpled, but then the test results are not replicable. Rolling the membrane forces the packaging into a cylindrical shape, but it avoids hard edges (360° folding). The membrane can be separated into multiple elements, which lie on top of each other when packed ("Stacked") and spread in different directions during deployment, like a flower.

There are endless ways of systematically folding the membrane and a few interesting folding techniques are listed below. An advantage of this packaging is that many shapes can be created to suit the volume restrictions.

Z-Folding

Like the form of "Z". Used, for example, for the ISS solar arrays (Fig. 2–2). For thicker membranes, material at the edges can be left out to reduce stress in the edges, as done in [42].

Fan

If one side of the Z-Folding has the same midpoint, it is a fan which has its elements side by side when stored, as seen in Fig. 2–4 for the MegaFlex and Fig. 3–1 for the Earwig.

A fan can also have the elements behind one another when stored, if the elements are only connected at the midpoint.

Map-Folding

If the Z-Folding is done in two axis directions it is called Map-Folding or rectangular

Miura-Ori. [43]

Miura-Ori

A specific Miura-Ori folding has already been mentioned when discussing the hornbeam/beech leaves in Chapter 3.1.1. The general folding process is shown in Fig. 3–9 and described in detail in [43] and [44]. It differs from Map-Folding because the angle between the folding lines is not 90° , which leads to the main advantage that an induced movement in one direction leads to a deployment in multiple directions.

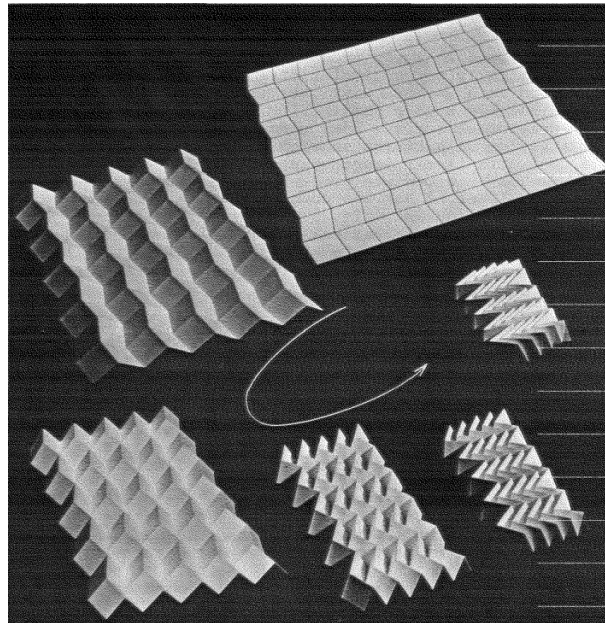


Fig. 3–9: Miura-Ori folding process [43]

Leaf-In Pattern

A Miura-Ori folding towards a mid-point is called “Leaf-In Pattern” in [44].

The final packaging can also be a combination of the above. Like the Gossamer-1 solar sail, which uses a Z-folding combined with rolling (see Fig. 2–7).

Wrapping around a Hub

A membrane can be wrapped around a hub as shown in Fig. 3–10 and described in [43]. OrigamiSat-1 will use the Wrapping around a Hub method with four tape springs as booms to deploy thin-film solar cells on a membrane [20, 45]. Other combinations of folding and rolling can be found in [42] and [46].

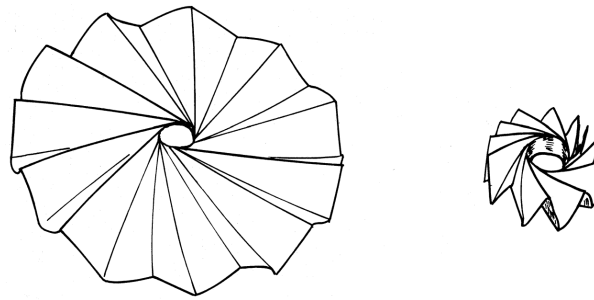


Fig. 3–10: Wrapping a membrane around a hub [43]

For most folding patterns, it is important to avoid folding multiple layers at once, because the thickness of the folded layer will multiply and the increased radius at the edge causes more stress. Little holes on the edges can reduce this stress.

The main advantage of Miura-Ori that an induced movement in one direction leads to a deployment in multiple directions, needs a certain stiffness of the membrane. This may not be achieved by the selected membrane, because it contradicts the lightweight design.

Z-Folding is the simplest and most efficient packaging method. It's folding is longitudinal in one direction, while Map-Folding is longitudinal folding regarding two directions. The Wrapped around a Hub pattern has a large bending radius, which can simplify the requirements for an integrated structure, but the positioning on the CubeSat is difficult, because it has to be able to deploy in all directions of its plain.

This shows that the main differences are the possible ways of deployment and the resulting packed volume. Therefore, folding pattern selection is dependant on the placement within the CubeSat, its volume constraints and a suitable deployment method.

3.1.5 Membranes

Since the exact application of the self-deploying membrane is not specified (base for solar cells, solar sail, drag sail, sunshield) the membrane characteristics are not specified either. The solution should be applicable for different membranes.

Typical membrane materials are: CP-1, CP-2, Polycarbonate, Kapton, Mylar.

An important partition is whether the material is a thermoplastic (deformable at certain temperatures) or thermoset (not deformable after curing). The fused polycarbonate used in tests in [6] (see Chapter 3.1.6) is a thermoplastic.

Another possibility, which is not further examined in this thesis, is to not use a thin film as membrane. For example, the stiffening structure itself and its deployment can be examined without a membrane, or a Microtruss Structure or a 3D-Regular Micro Structure can replace the membrane [6].

3.1.6 Rip-Stop

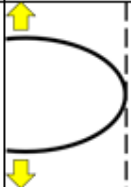

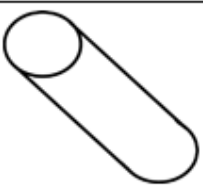


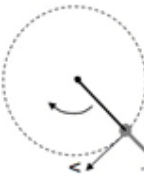
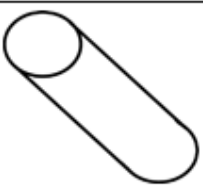





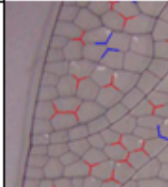

A hole inside a tensioned membrane propagates quickly. To stop the whole membrane from ripping apart after being hit by a micrometeor or space debris, a rip-stop method has to be applied. One example for a rip-stop can be found on the sunshield membranes of the JWST, where layers of the membrane and reinforcing stripes are thermally bonded together. These “Thermal Spot Bondings” form a grid pattern and keep a rip within the given grid area. [23]

Tests about polycarbonate rip-stop patterns on a polycarbonate membrane applied by fused deposition manufacturing can be found in [6].

Rip-stop can be seen as a very thin stiffening structure and its pattern is equally derived from nature. Therefore decisions about it are made after the concept for membrane stiffening is more advanced and rip-stop is not listed in the morphological box.

3.2 Morphological Box

An extensive list of the previously described partial solutions is given in Tab. 3–1.

Solution / Category		1	2	3	4	5	6	7	8	9
A. Deployment Method	Tensed Structure		Boom		Inflation	Shape Memory Alloy	Electroactive Polymers	Motor	Electromagnetic Repulsion	Centrifugal Forces
	Mini Rods			Rigidizing			Membrane Shape	Membrane Taut Frame	Cable Harness	
B. Stiffening Structure										
C. Distribution of Stiffening Structure	Insect Wing (Cells)		Bat Wing (Hinges & Taut Membrane)	Spider Web (Circular)	Leaf (Branching)	Regular Mesh	Irregular Mesh	None		
D. Packaging	Folding		Rolling	Combination	Stacking	Crumpled				

Tab. 3–1: Morphological Box. Picture source Chapter 3.1 or [6, 47, 48, 49, 50, 51, 52]



3.3 Combination of Concepts

In this section, partial solutions from the morphological box are combined in a way that the partial solutions harmonize, to create whole concepts fulfilling the requirements in the best possible way. The combinations are shown in Tab. 3–2, followed by a description of each concept. These concepts are evaluated in the following section.

Category: Concept:	Deployment Method	Stiffening Structure	Distribution	Packaging
EAP Bat	Electroactive Polymers	Membrane Taut Frame	Bat Wing	Folding
Taut SMA	Shape Memory Alloy	Shape Memory Alloy	None	
Cable Repulsion	Electromagnetic Repulsion	Cable Harness	Regular Mesh	Folding
Rigidized Web	Centrifugal Forces	Rigidizing	Spider Web	Combination
Tensed around a Hub	Tensed Structure	Mini Rods	Spider Web	Combination
Flower	Tensed Structure	Mini Rods	Spider Web	Stacking and Folding
Beetle	Tensed Structure	Mini Rods and Membrane Shape		Folding
Leaf	Tensed Structure and Booms	Mini Rods and Booms	Leaf	Rolling
Inflated Leaf	Inflation	Inflation	Leaf	
Rectangles	Tensed Str. and Tape Springs	Mini Rods and Booms	Insect Wing	Folding
Double Folded Fan	Tensed Structure	Mini Rods	Insect Wing	Folding

Tab. 3-2: Concept Combination Matrix

EAP Bat

Deployment Method:	A6	Electroactive Polymers
Stiffening Structure:	B7	Membrane Taut Frame
Distribution:	C2	Bat Wing
Packaging:	D1	Folding

The membrane is folded on the outside of a CubeSat until deployment through EAP. EAP is also called artificial muscle and can imitate the muscular deployment of a bat wing. After deployment, the membrane is taut within the frame that looks like an abstraction of the bones of a bat wing.

Alternatively, a Motor (A7) can be used to pull a bowden cable connected to the structure.

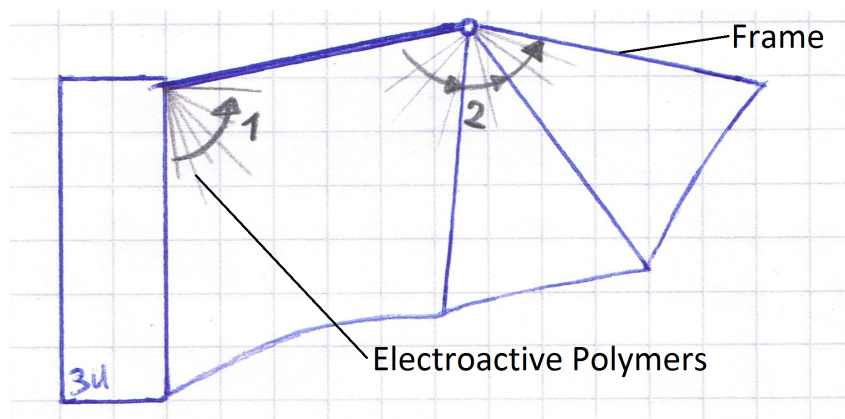


Fig. 3–11: Concept: EAP Bat

Advantages and Disadvantages:

- + Low level of complexity for stiffening and deployment movement (not for EAP)
- + Membrane orientation (relative to the spacecraft) is moderately adjustable at one joint
- High development effort for this application of EAP
- Low packaging efficiency
- The concept reminds of MegaFlex (see Chapter 2.2)
- Hardly adaptable to size, packaging and placement requirements

This concept is not very efficient and EAP has a low TRL.

Taut SMA

Deployment Method:	A5	Shape Memory Alloy
Stiffening Structure:	B5	Shape Memory Alloy
Distribution:	C7	None
Packaging:	D	Variable

A SMA within the outer edge of the packed membrane (see Fig. 3–12) gets heated by an electrical current during deployment. This makes the SMA return to its original shape, a circle/oval which is slightly larger than the membrane, so that the membrane gets stretched and stays flat. No additional stiffening structure, but a Rip-Stop pattern is needed.

The way the membrane should be stored depends on the deployment behavior of the SMA. After opening the compartment, it has to be ensured that the membrane and SMA does not block itself from full deployment.

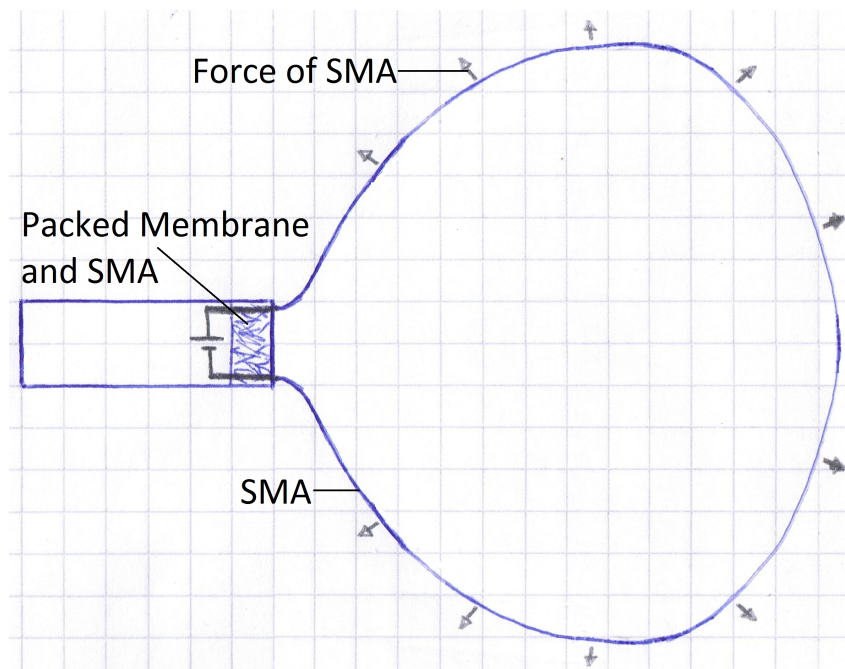


Fig. 3–12: Concept: Taut SMA

Advantages and Disadvantages:

- + Large membrane area
- + Lightweight
- + Low level of complexity
- + Easily adaptable to size, packaging and placement requirements
- + Membrane orientation is adjustable at one complex joint
- Medium-High risk of deployment being stuck

Cable Repulsion

Deployment Method:	A8	Electromagnetic Repulsion
Stiffening Structure:	B8	Cable Harness
Distribution:	C5	Regular Mesh
Packaging:	D1	Folding

The wires used for the solar cells are integrated into the membrane to provide stiffness. After Z-Folding the membrane, the wires lie on top of each other and a special electrical circuit results in an electromagnetic repulsion to deploy the membranes.

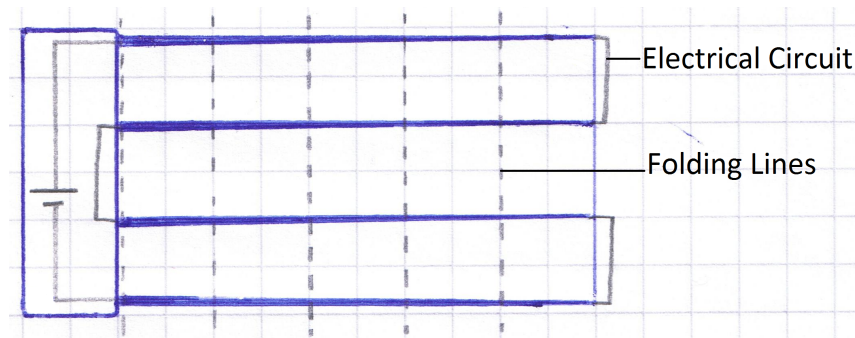


Fig. 3–13: Concept: Cable Repulsion

Advantages and Disadvantages:

- + Possibility of mass reduction by using existing electrical wires as stiffening and deployment method
- Deployment hardly testable
- Complex positioning of solar cells and wires on the membrane
- Electromagnetic repulsion is likely not able to deploy by 180° (Large flatness deviations)
- The wire characteristics are probably different from the required stiffening characteristics
- Hardly adaptable to packaging and placement requirements
- Membrane orientation is not adjustable

Rigidized Web

Deployment Method:	A9	Centrifugal Force
Stiffening Structure:	B3	Rigidizing
Distribution:	C3	Spider Web
Packaging:	D3	Combination

A circular membrane with a stiffening and rip-stop pattern, like a spider web, is packed in the “Wrapped around a Hub” method (see Fig. 3–10). The spacecraft, or only the membrane subsystem, spins to deploy the membrane through centrifugal forces. Then the stiffening pattern, made out of a special material, rigidizes in the sunlight. After a specific stiffness is reached, the spacecraft can stop spinning without collapsing the membrane.

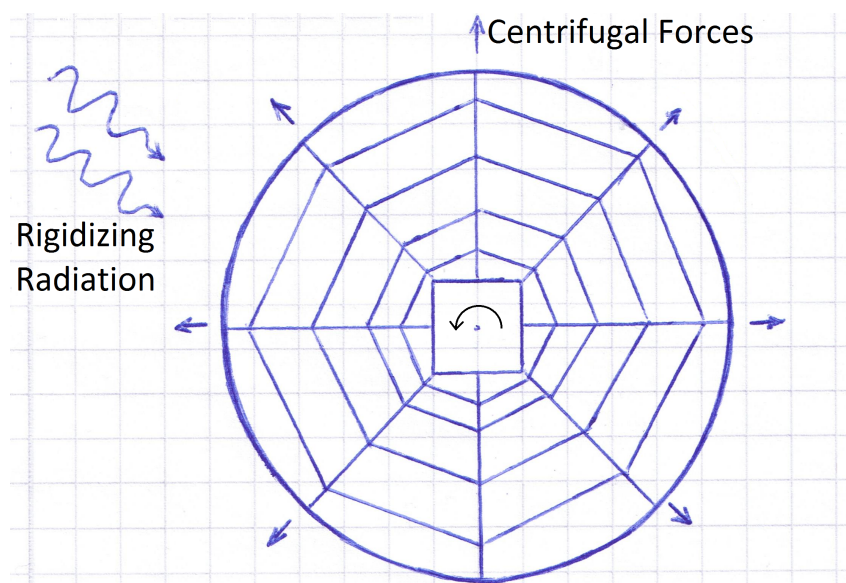


Fig. 3–14: Concept: Rigidized Web

Advantages and Disadvantages:

- + Easy deployment method
- + No mass needed for a deployment mechanism
- + The Center of Gravity (CG) is in the center of the satellite and the membrane is distributed evenly around it
- + Membrane orientation is adjustable at one joint
 - Satellite or subsystem has to spin
 - Satellite could be inoperable during the spinning/rigidizing time
 - Applicable rigidizable materials have not yet been studied
 - Low packaging efficiency
 - Flatness deviations

Tensed around a Hub

Deployment Method:	A1	Tension
Stiffening Structure:	B1	Mini Rods
Distribution:	C3	Spider Web
Packaging:	D3	Combination

Like a Rigidized Web, a circular membrane with a stiffening and rip-stop pattern is packed in the “Wrapped around a Hub” method (see Fig. 3–15). The stiffening is done by flexible mini rods on some folding-element. When packed, these mini rods are wrapped around the hub (with a larger bending radius than for most other folding methods, which simplifies the rod requirements) and tensed. After release this tension deploys the membrane.

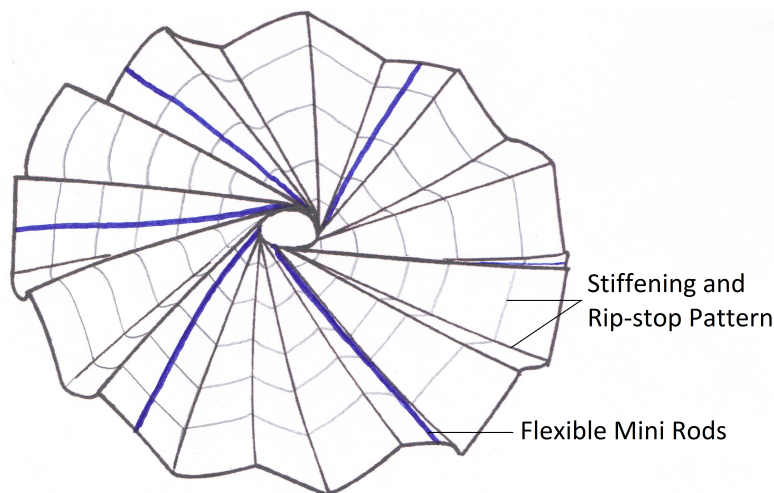


Fig. 3–15: Concept: Tensed around a Hub. Edited from [43]

Advantages and Disadvantages:

- + Easy deployment method
- + Low development effort expected
- + The CG is in the center of the satellite and the membrane is distributed evenly around it
- + Membrane orientation is adjustable at one joint
- Low packaging efficiency
- Flatness deviations

Flower

Deployment Method:	A1	Tension
Stiffening Structure:	B1	Mini Rods
Distribution:	C3	Spider Web
Packaging:	D4 D1	Stacking and Folding

The membrane is folded and stacked against the outside of the CubeSat together with four mini rods attached to the bottom of the CubeSat. When released, these rods turn by 90° (see the movement marked with "1" in Fig. 3–16) and the second half of the rod is free to deploy by 180° (see the movement marked with "2" in Fig. 3–16). This works either by very flexible rods, self-deploying hinges within the rod (A3), a shape memory alloy (A5) or a motor (A7) pulling on bowden cables to deploy not-self-deploying hinges. After deployment, the stiffness is provided by these rods, together with smaller rods integrated into the membrane. Alternatively, the rods are a taut frame to the membrane without integrated stiffening structure (B7 + C7).

The rods can be next to the rails, or parts of the rails can become the deployed rods.

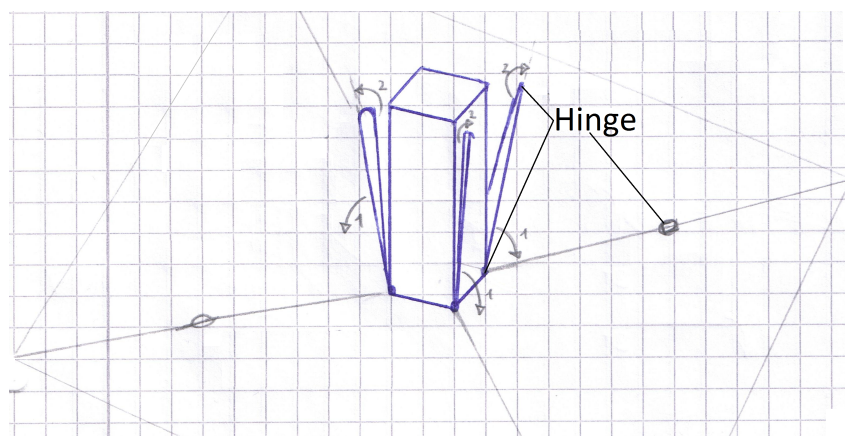


Fig. 3–16: Concept: Flower

Advantages and Disadvantages:

- + Low flatness deviations
- The concept is similar to the Typical Sail Architecture with rods as booms
- Packed membrane occupies most of the satellite surface and needs an additional cover (increases mass)
- Membrane orientation needs four adjustable joints

Beetle

Deployment Method:	A1	Tension
Stiffening Structure:	B1 B6	Mini Rods and Membrane Shape
Distribution:	C	Variable
Packaging:	D1	Folding

The beetle folds its wing into half twice and the resulting angle in the middle is less than 360° . This is a stiffening mechanism through the membrane shape, which has been described for the Earwig (3.1.1). An abstraction of the beetle wing has been sketched in Fig. 3–17. More elements can be added on either side. This stiffening method will be paired with mini rods integrated into the membrane and deployment through tension.

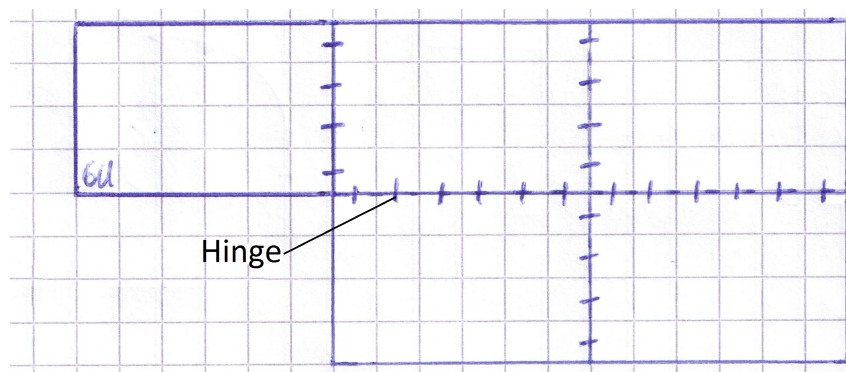


Fig. 3–17: Concept: Beetle

Advantages and Disadvantages:

- + Easily adaptable to size and packaging requirements (by adding/leaving out elements)
- + Large membrane size possible
- Low stiffness for large sizes
- Flatness deviations get amplified, because the membrane is not built concentric or with a stiff main rod/tape spring
- Hardly adaptable to placement changes (needs a large base area)
- The concept is similar to typical rigid solar arrays
- Membrane shape stiffening works only in one direction
- Membrane orientation is not adjustable

Leaf

Deployment Method:	A1 A2	Tension and Boom
Stiffening Structure:	B1 B2	Mini Rods and Boom
Distribution:	C4	Leaf
Packaging:	D2	Rolling

Imitating a leaf led to the left sketch of Fig. 3–18. The “primary vein” is a tape spring, the “secondary veins” are thick mini rods ending in a hinge and the “tertiary veins” are small mini rods distributed over the whole membrane. The whole membrane will be rolled and deployed through the boom and tension in the hinges.

The sketch on the right side shows a stronger abstraction of the leaf. The area of the membrane is larger and modified to occupy the whole CubeSat side area, when folded, for a more efficient volume usage.

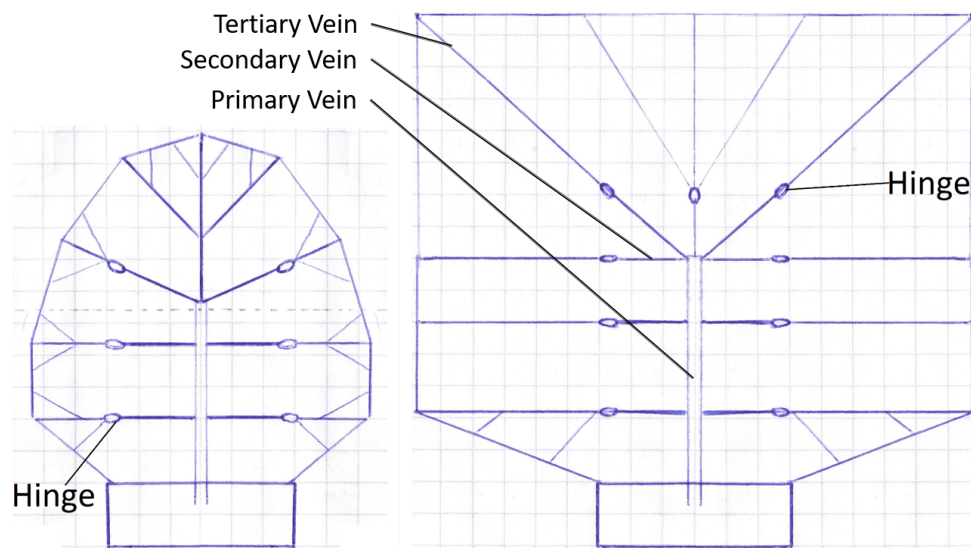


Fig. 3–18: Concept: Leaf

Advantages and Disadvantages:

- + Membrane orientation can be adjustable at one joint
- Efficient placement of a cylinder (rolled up membrane) is difficult

Inflated Leaf

Deployment Method:	A4	Inflation
Stiffening Structure:	B4	Inflation
Distribution:	C4	Leaf
Packaging:	D	Variable

The vein structure of a leaf can be adapted for the use of inflatables. The sketch in Fig. 3–19 shows inflatable channels arranged in a simplification of the Jackfruit leaf veins (see Fig. 3–6). During deployment, these channels get pressurized and extended, pulling the membrane out and stretching it.

The channels can be manufactured with an additional tube within or on the membrane (increases mass), or by joining two layers of the membrane, while cavities form the channels (peel stress).

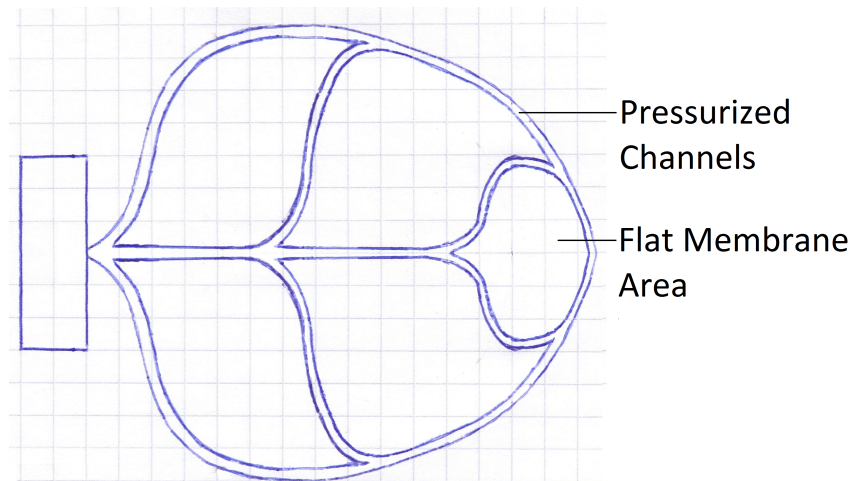


Fig. 3–19: Concept: Inflated Leaf

Advantages and Disadvantages:

- + Simple principle
- + Easily adaptable to placement and packaging requirements
- + Membrane orientation is adjustable at one complex joint
- Risk of destruction by depressurization (e.g. by random micrometeorite impact)
- Additional mechanism (and its mass) for pressurization

Rectangles

Deployment Method:	A1 A2 A3	Tension, Tape Spring Hinge and Boom
Stiffening Structure:	B1 B2	Mini Rods and Boom
Distribution:	C1	Insect Wing
Packaging:	D1	Folding

As in the Leaf Concept, tape springs are used as primary stiffening along with mini rods in an insect wing pattern (see Fig. 3–20). First, three layers of the membrane are deployed out of a Z-folded state by the tape springs. Then, one layer is deployed to the left side and one to the right side to tripple the overall membrane area. This is done along a line of hinges next to the tape spring. It is not specified which hinge type will be used (Tape Spring Hinge (A3), O-Hinge or a different tensed method (A1)).

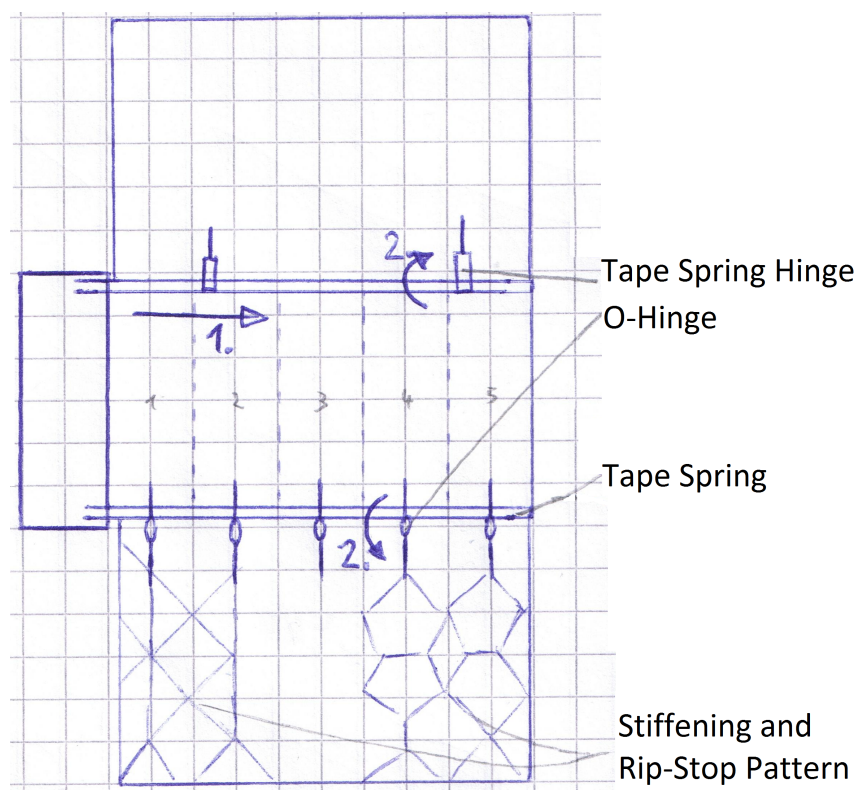


Fig. 3–20: Concept: Rectangles

Advantages and Disadvantages:

- + Different hinges applicable
- + Easily adaptable to size and packaging requirements
- Not adaptable to changes in accomodation on the satallite
- Mass and volume increase due to the Tape Spring
- Membrane orientation is not adjustable

Double Folded Fan

Deployment Method:	A1	Tension
Stiffening Structure:	B1	Mini Rods
Distribution:	C1	Insect Wing
Packaging:	D1	Folding

This concept is inspired by the Earwig, which fanfolds its wing and in the next step folds it into half. This is shown in Fig. 3–21 a) and leads to an increased bending radius and area. Doing this the other way around as shown in Fig. 3–21 b) would lead to a membrane folding at the base of the fan that is challenging to realize.

Fig. 3–21 c) shows the application of this. On opposing sides of a CubeSat, the upper half of the fan is deployed first, and it is then unfolded along the angle α . The value of α depends on storage volume and required membrane area.

The fan is stiffened by mini rods along each fan element. The rods should be placed alternately for a more efficient packing. At the doubling-folding line, the rod becomes an O-Hinge, which has to be longer for every element (because the outermost element is bending around the other layers when stored, it has the largest bending radius and needs a larger O-Hinge than the first element).

The opening of the fan can be actuated by O-Hinges at the outer edge of the fan (as shown in Fig. 3–21), by a tape spring or torsion spring at the base of the mini rods. A membrane shape, for example realised by a fan element deployment of 175° instead of 180° , can stiffen the membrane further (B6).

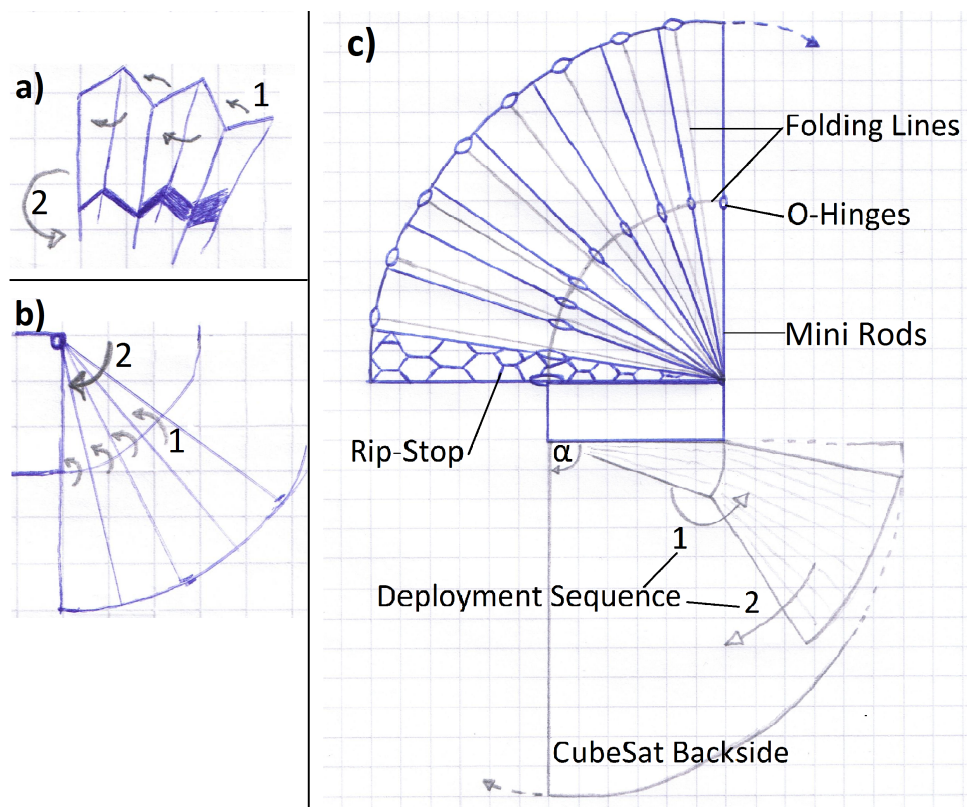


Fig. 3–21: Concept: Double Folded Fan

Advantages and Disadvantages:

- + Easily adaptable to size and packaging requirements
- + Large membrane size possible
- + Membrane orientation is adjustable at one joint
- Not adaptable to placement changes
- Many length variations of elastic hinges needed

3.4 Evaluation

Here the created concepts are compared and rated¹ in an evaluation matrix in Tab. 3–3. Each evaluation criterion is given points for each concept from 0 (bad) to 10 (good). These points are multiplied with the weighting factor and summed for the concept.

¹ The mean value of the ratings of Jannic Voelker and Martin Zander is given.

Evaluation Matrix (Technology Assessment)									
Average Rating of Jannic Voelker and Martin Zander									
Evaluation Criterion		Property parameter	EAP Bat			Taut SMA			
No. i	Weighting Factor g_i		Property e_{i1}	Value w_{i1}	Weighted Value wg_{i1}	Property e_{i2}	Value w_{i2}	Weighted Value wg_{i2}	
1	High Innovation Grade		Innovation grade	High	8	2,4	Medium	5	1,5
2	Low Effort of Realization (Manufacturing, Costs, Technically Possible)		Effort	Low	2	0,2	Medium	6	0,6
3	Low Complexity (Influence on Robustness & Reliability, Costs, Producability)		Complexity	Medium	4	0,2	High	7	0,35
4	Low Areal Density (Mass/Area, Mass Efficiency)		Areal Density [kg/m ²]	Medium	5	0,25	High	9	0,45
5	High Packaging Efficiency (Volume Efficiency)		Packaging Efficiency	Medium	5	0,75	High	8	1,2
6	Large Possible Membrane Size		Size [m ²]	Low	2	0,3	High	8	1,2
7	High Flatness		Flatness	Medium	4	0,4	High	7	0,7
8	High Stiffness		Stiffness [Nm ²]	High	7	0,7	Medium	4	0,4
Summe: $\sum g_i =$					$\sum wg_{i1} =$	5,2		$\sum wg_{i2} =$	6,4

Tab. 3–3: Evaluation Matrix

Cable Repulsion			Rigidized Web			Tensed around a Hub			Flower			Beetle		
Property	Value	Weighted Value	Property	Value	Weighted Value	Property	Value	Weighted Value	Property	Value	Weighted Value	Property	Value	Weighted Value
E_{i3}	w_{i3}	wG_{i3}	E_{i4}	w_{i4}	wG_{i4}	E_{i5}	w_{i5}	wG_{i5}	E_{i6}	w_{i6}	wG_{i6}	E_{i7}	w_{i7}	wG_{i7}
High	8	2,4	High	7	2,1	Medium	4	1,2	Low	2,5	0,75	Medium	5	1,5
Low	1	0,1	Low	3	0,3	High	8	0,8	Medium	6,5	0,65	Medium	5,5	0,55
Low	2	0,1	High	7	0,35	High	7,5	0,375	High	7	0,35	Medium	6,5	0,325
High	9	0,45	High	7	0,35	High	7	0,35	High	7	0,35	Medium	5	0,25
High	7	1,05	Low	3	0,45	Medium	4	0,6	Medium	5	0,75	High	8,5	1,275
Medium	6	0,9	Medium	4	0,6	Low	3	0,45	Low	3	0,45	High	7,5	1,125
Low	1	0,1	Low	3	0,3	Medium	3,5	0,35	High	8	0,8	Medium	4	0,4
Low	2	0,2	Medium	6	0,6	Medium	4	0,4	Medium	4,5	0,45	Low	3	0,3
$\Sigma wG_{i3} = 5,3$			$\Sigma wG_{i4} = 5,05$			$\Sigma wG_{i5} = 4,525$			$\Sigma wG_{i6} = 4,55$			$\Sigma wG_{i7} = 5,725$		

Leaf			Inflated Leaf			Rectangles			Double Folded Fan		
Property	Value	Weighted Value	Property	Value	Weighted Value	Property	Value	Weighted Value	Property	Value	Weighted Value
E_{i8}	W_{i8}	$W_{G:8}$	E_{i9}	W_{i9}	$W_{G:9}$	E_{i10}	W_{i10}	$W_{G:10}$	E_{i11}	W_{i11}	$W_{G:11}$
High	8,5	2,55	High	7	2,1	High	7	2,1	High	9	2,7
Medium	5	0,5	Medium	5	0,5	Medium	6	0,6	Medium	5,5	0,55
Low	3	0,15	High	7	0,35	High	7	0,35	Medium	6	0,3
Medium	4	0,2	Medium	4	0,2	Medium	4	0,2	High	8	0,4
Medium	6	0,9	High	8,5	1,275	High	7	1,05	High	7,5	1,125
Medium	5,5	0,825	High	7	1,05	Medium	6	0,9	High	8	1,2
Medium	6	0,6	High	7	0,7	High	8	0,8	Medium	5	0,5
High	7	0,7	Medium	5,5	0,55	High	7,5	0,75	High	7	0,7
$\Sigma W_{G:8} =$		6,425	$\Sigma W_{G:9} =$		6,725	$\Sigma W_{G:10} =$		6,75	$\Sigma W_{G:11} =$		7,475

Evaluation Matrix Part 3

The concepts “Flower” and “Tensed around a Hub” have the lowest overall rating. This is mainly because of a low innovation grade, which is accompanied by a low effort of realisation. For the “Tensed around a Hub” concept, only flexible rods with a big bending radius have to be joined with a membrane. The expected low flatness, low stiffness and small size, however, make this concept uninteresting. “Flower” is very similar to the typical sail architecture. The difference is that “Flower” uses flexible rods instead of booms and stores the membrane on the outside of the satellite.

“EAP Bat”, “Cable Repulsion” and the “Rigidized Web” are not developed further in this thesis, because they have a high effort of realisation, while the other evaluation criterions are in the medium range.

“Inflated Leaf” and “Taut SMA” have good ratings and a particularly high packaging efficiency. This is because of their deployment concepts, which do not need a complicated sequence of movements, but can deploy a randomly folded membrane in a single action - as long as it does not get stuck within the satellite. The “Taut SMA” concept is expected to be lightweight and therefore, the membrane size can be large. The main disadvantage of the “Inflated Leaf” concept is the ever-present risk of depressurization, for example, by a micrometeorite or space debris impact on a pressurized channel. A countermeasure could be additional rigidizing of the channels (B3), so that after a while, the stiffness of the membrane is not pressure dependent. However, as mentioned in Chapter 3.1.2, [22] examined inflation for membrane deployment and was not successful.

The best rated concepts are “Double Folded Fan”, which has a low areal density and, therefore, a large possible membrane size, and “Rectangles”, which is expected to have a high flatness.

Just like “Leaf” (high innovation grade) and “Beetle” (high packaging efficiency), they rely on tensed mini rods, which can be folded 180° like an elastic hinge. Such small elastic hinges, however, do not exist. An applicable example is the O-Hinge (Earwig, see Chapter 3.1.1), but O-Hinges have been tested only once in a simple manner in [6]. This is not sufficient as a basis for further development, considering its functionality is a single point of failure for all four concepts. Tape Spring Hinges (examined in [33]) are an alternative to O-Hinges, but since they are estimated to be more complex and have more mass than elastic hinges, the applicability of elastic hinges shall be examined first.

Instead of selecting a concept for detailed design, not knowing if the elastic hinge will work as intended, this thesis focuses on investigating the “Hinge” itself. The objective is a proof of concept, and developing a standard element of the Hinge, which can be implemented in any of these concepts at a later point.

4 Elastic Hinge - Design and Test

In this chapter, different designs for elastic hinges are presented and evaluated, based on tests during rapid prototyping. The main design drivers are the stability and the angle between its rods after deployment (optimal: 180°). The most promising design is selected for an optimization by FEM analysis and parametrisation in the next chapter.

For the manufacturing process the Additive Layer Manufacturing (ALM) technique was selected, because of the possibility to print directly on the membrane (so that it is already jointed), and because of the fast production times for individual specimen. The usability (printing method, precision) of the available 3D Printers at DLR are examined. Favorable material characteristics will be identified as a starting point for the optimization by FEM analysis.

Please note that the Hinge is printed and examined without a membrane during the rapid prototyping. Manufacturing of a detailed design on a membrane will be undertaken by NASA at a later point, just like development of the necessary manufacturing resources and an appropriate material.

4.1 Designs

During the rapid prototyping process, designs for Hinges have been improved, eliminated and newly-created. The best final designs are described in this section.

Rod

A simple rod without changes in geometry at the folding lines is used as a baseline for comparison. This design can be applied to very small rods, like for the Rip-Stop structure.

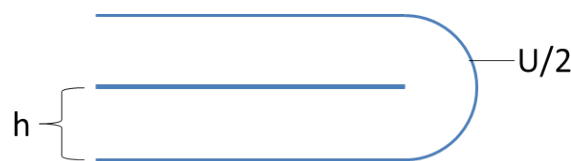


Fig. 4–1: Design: Bent Rod

The thickness of the rod (h) is its outer bending radius (r) ($U/2 = \pi \cdot r = \pi \cdot h$). The inner bending radius is nearly 0. The stress in the rod increases with the difference between the inner and outer bending radii. The greater the difference, the larger the required yield elongation of the material, for the deformation to stay in the elastic region. If plastic deformation occurs, one side of the rod is permanently elongated and, after release, it will not deploy by a full 180° .

There are three different ways to avoid plastic deformation:

- Finding a material with a high Yield Elongation
- Reducing the Bending Radii Difference by design variations
- Changing from bending to torsion

The necessary yield elongation is very large (about 300%). However, the material has to fulfill other, more important requirements, like space qualification and manufacturability. Finding a material that fulfills these requirements and has a very high yield elongation is unlikely. Therefore, the other options, reducing the bending radii difference and changing from bending to torsion, are examined here.

4.1.1 Reducing the Bending Radii Difference by Design Variations

Wide and Flat-Hinge

By reducing the thickness of the rod (h), the difference in bending radii is decreased. To avoid creating a weak spot in the rod, the width is increased so that the cross section area stays the same.

The Hinge is shown in Fig. 4–2, with its folding axis and an arrow indicating the folding direction. The rod cross section is 1 mm * 1 mm and the fold-part is 3 mm wide and 0.33 mm flat. All CAD Files and Figures in this chapter have a 1 mm * 1 mm rod cross section.

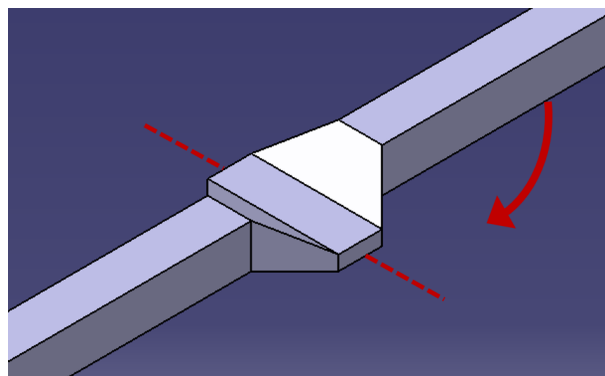


Fig. 4–2: Design: Wide and Flat-Hinge

Advantages and Disadvantages:

- + Simple geometry
- Bends only in one direction (towards the wide and flat side)
- Significantly reduced stiffness in the folding/deployment direction

Bowl-Hinge

The Bowl-Hinge is shown in Fig. 4–3, with its folding axis and arrows indicating the folding direction. There is no indication in the following design figures, because the Hinge orientation is unchanged.

When bent, the outer walls spread to the sides to decrease the bending radius. The spread walls increase the Reopening-force (compared to no walls). The principle is similar to that of the Tape Spring Hinge.

Detailed pictures of the folding of a Bowl-Hinge can be found in Appendix A.3.

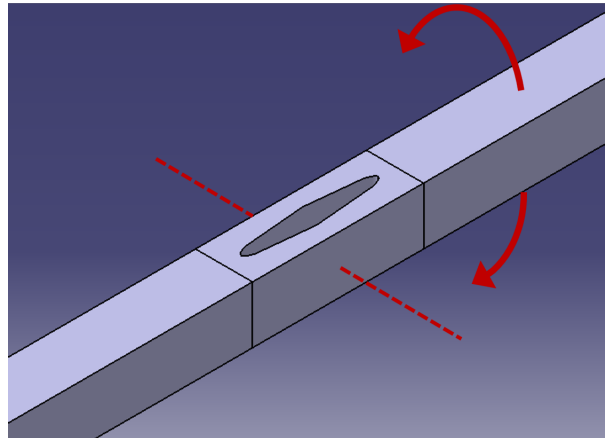


Fig. 4–3: Design: Bowl Hinge

Advantages and Disadvantages:

- + A wide range of variations is possible, with a possible transition to Tape Spring Hinges
- Very thin walls limit the minimum size and are prone to rips

O-Hinge

The already mentioned O-Hinge imitates the Earwig and has a split rod, which forms an O. Two points of bending instead of one means that the cross section of each rod is smaller, which decreases the difference in bending radii.

Detailed pictures of the folding of a O-Hinge can be found in Appendix A.4.

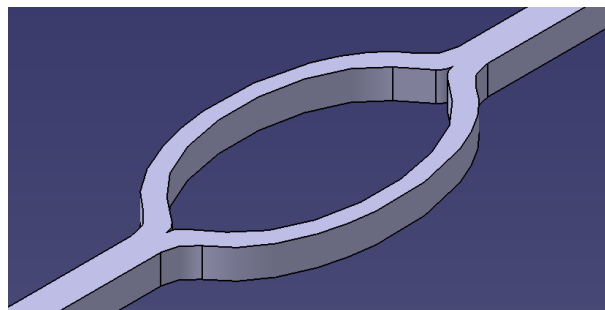


Fig. 4–4: Design: O-Hinge

Advantages and Disadvantages:

- + Rods don't need to be perfectly aligned for bending
- A section of the "O" breaks before the big rod would

Stretching-O-Hinge

This is a special case of the O-Hinge geometry, where the sides stretch away from the middle point when folded. This displacement elongates the bent path, which increases the bending radius and thus reduces the tension.

Advantages and Disadvantages:

- + If it is connected to a membrane, bending will stretch it, which is an additional Reopening-force. A simplified view is an O-Hinge with its sides connected by a spring
- The membrane could stop the Hinge from bending at all

A design that achieves this effect has not yet been found.

4.1.2 Changing from Bending to Torsion

Torsion-Hinge

The Torsion-Hinge, shown in Fig. 4–5, translates the bending to torsion. The length of the twisted rod (subsequently called the "Torsion-Rod") can be adjusted, with material characteristics and folding requirements. The left image in Fig. 4–5 shows small Torsion-Rods for soft material, while the right image shows long Torsion-Rods for hard materials.

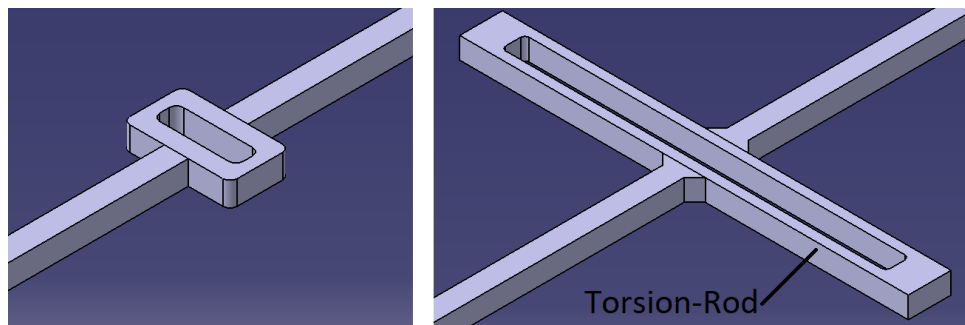


Fig. 4–5: Design: Torsion-Hinges

Advantages and Disadvantages:

- + The Torsion-Rod length is adaptable to material properties
- The distance between the Torsion-Rods remains constant when folded

Oval-Hinge

A combination of the O-Hinge and Torsion-Hinge is the Oval-Hinge. It combines bending and torsion movement to store the deployment energy.

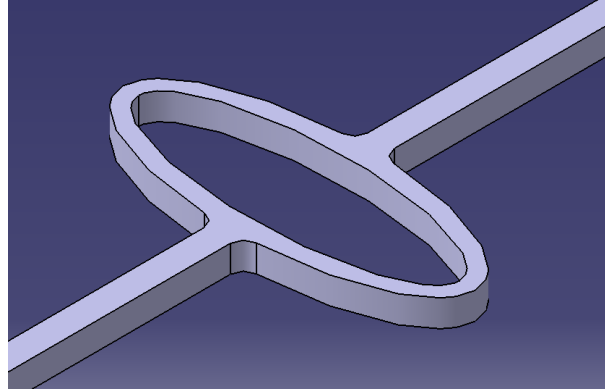


Fig. 4–6: Design: Oval-Hinge

Advantages and Disadvantages:

- + Good adaptability to material properties
- More complicated geometry than the Torsion-Hinge (especially, when bent)

4.1.3 Multiple Material Designs

Using two different materials for the Hinge can be very helpful, since the functions of the rod and the Hinge are very different. Every listed Hinge can change the material of sections to a more flexible one. The two designs with the best test results are listed below. Fig. 4–7 and Fig. 4–8 show the rod with stiff material colored grey and the Hinge with flexible material colored yellow. More tested designs are described next to the tests in Chapter 4.3.3.

O2-Hinge

The previously described O-Hinge gets two long sections of flexible material as shown in Fig. 4–7.

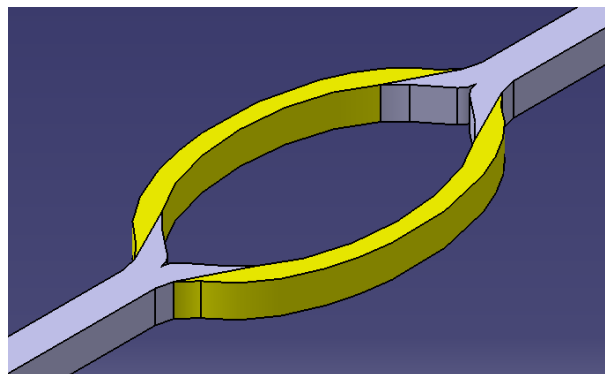


Fig. 4–7: Design: O2-Hinge

Advantages and Disadvantages:

- + Rods don't need to be perfectly aligned for bending
- A section of the "O" breaks before the big rod
- The flexible material reduces overall stiffness
- Possibility of a weak spot at the connection between the stiff and the flexible material

Filled-O-Hinge

The "O" is filled with flexible material to increase the overall stiffness, resistance against breaking and Reopening-for. This is a close replication of the Earwigs O-Hinge, which is mostly made of resilin (see Chapter 3.1.1 and Fig. 3–2). The area of the connection between stiff and flexible material is larger than for the O2-Hinge, which makes it less likely to be a weak spot.

This Hinge can be combined with the Wide and Flat-Hinge, by making the Filled-O thinner. However, this would reduce the stiffness in the folding/deployment plane.

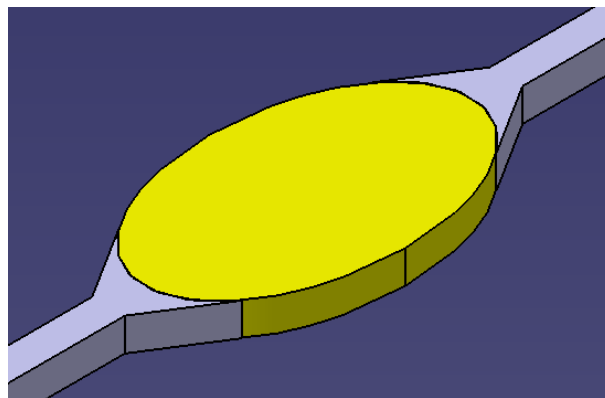


Fig. 4–8: Design: Filled-O-Hinge

Advantages and Disadvantages:

- + Can connect more than two rods
- + Rods don't need to be perfectly aligned for bending
- + "O" has no weak spots for breaking/rip-propagation
- The flexible material reduces overall stiffness
- Larger mass

4.2 3D Printer and Materials

For printing of these designs, the 3D printers listed in Tab. 4–1 were available at the Institute of Composite Structures and Adaptive Systems (IFA) at DLR. Every printer was used to test its precision, printing method and its printable materials. The results are listed in the following subsections.

Company	3D Printer	Feature	Method	Nozzle-Diameter	Layer-Resolution	Tested Materials
MakerBot	Replicator+		FDM	0.4 mm	0.1 mm	PLA & Tough PLA
Prusa	Prusa i3 MK2		FDM	0.4 mm	0.05 mm	PLA, ABS, PETG, Flex
Formlabs	Form 2	High Precision	SLA	0.14 mm	0.025-0.1 mm	Flexible, Durable, Tough, High Temp
Markforged	Mark Two	Fiber Insertion	FDM	0.4 mm	0.1 mm	Onyx, Nylon, Nylon + HSHT Fiberglass
Stratasys	Objet260 Connex3	Mixing Materials	MJM	0.2 mm	0.016 mm	see Chapter 4.3.3

Tab. 4–1: 3D Printer Characteristics and Materials [53, 54, 55, 56, 57]

4.2.1 Precision

Small Hinges (1 mm rod height) printed with the Replicator+ or Mark Two turned out to be too inaccurate for the needed small scale. Since the Prusa printer had a good accuracy, the Layer Resolution is more important than the nozzle diameter (see Tab. 4–1). So for an estimated Hinge size of 1 mm² rod cross section, the following printer requirements are recommended:

Nozzle Diameter ≤ 0.4 mm

Layer Resolution < 0.1 mm

However, the exact size of the Hinges and structures is not determined yet. A rip-stop structure, which will be printed on the membrane, may be even smaller and require a more precise printer.

4.2.2 Method

Regarding the Method, FDM with multiple different materials should be used, because it is the simplest method to print on a membrane. In Stereolithography (SLA), the print is done inside resin and needs cleaning and hardening as further treatments. Even though the structure could be printed on a membrane, while it is inside the resin, the manufacturing would be more complex than FDM. Prints from the Objet260 need to be separated from the supporting material as treatment after printing. Then, they would have to be attached to the membrane. This increases the complexity of manufacturing drastically and is expected to produce a weaker bonding. However, a MultiJet Modeling (MJM) method without the excessive use of supporting material may be preferable over FDM, because of a higher precision and material mixing.

4.2.3 Material Properties

In Tab. 4–2 and Tab. 4–3, the material properties of the materials with the best test results are listed. These properties are related to test results in the following sections and especially in Chapter 5. The materials are not space qualified (see Requirement G6 in Chapter 1.2.1.2).

The datasheets rarely provide all important properties and their details differ from one another (see footnotes of Tab. 4–2). Therefore, some cells in the tables are empty and comparing the materials is difficult.

Objet260 Connex3:

RGD stands for rigid, FLX for flexible. VeroCyan and RGD525 are rigid materials, Agilus30 Black and TangoBlack+ are flexible materials. The materials listed in between two of these in Tab. 4–3 are mixtures of these two. Stratasys provides no material characteristics for RGD K60 and RGD K50.

Printer	Form 2		Mark Two
Material	Durable	Flexible	Nylon
Tensile Strength [MPa]	31.8	7.7-8.5	54 ¹
Tensile Modulus [MPa]	1260		940
Tensile Elongation at Break [%]	49	75-85	260 ²
Flexural Strength [MPa]	27.2 ³		32
Flexural Modulus [MPa]	820		840

Tab. 4–2: Material Properties 1 [58, 59, 60]

¹ 31 MPa at Yield

² 27 % at Yield

³ at 5% Strain

Printer	Objet260 Connex3									
Material	TangoBlack+	FLX9640	FLX9650	FLX9660	FLX9670	FLX9685	FLX9695	RGD5250	RGD5225	RGD525
Tensile Strength [MPa]	0.8-1.5	1.3-1.8	2-2.8	2.8-4	3.8-4.9	6-7.3	9-12	50-56	43-55	70-80
Tensile Modulus [MPa]								1700-2400	1600-2700	3200-3500
Flexural Strength [MPa]								47-70	50-100	110-130
Flexural Modulus [MPa]								1400-2000	1700-2700	3100-3500
Elongation at Break [%]	170-220	100-130	80-100	60-80	50-70	35-50	27-40	18-27	9-15	10-15
Tensile Tear Resistance [kg/cm]	2-4	5-7	8-10	10.5-12.5	13-15	22.5-24.5	45-47			
Material	Agilus30 Black	FLX9740	FLX9750	FLX9760	FLX9770	FLX9785	FLX9795	RGD K50	RGD K60	VeroCyan
Tensile Strength [MPa]	2.4-3.1	3-4	3-4	3.5-4.5	4-6	6-10	10-14			50-65
Tensile Modulus [MPa]										2000-3000
Flexural Strength [MPa]										75-110
Flexural Modulus [MPa]										2200-3200
Elongation at Break [%]	220-240	190-210	170-210	150-170	120-140	70-90	50-70			10-25
Tensile Tear Resistance [kg/cm]	5-7	6-8	7-9	7-10	12-14	22-26	26-30			

Tab. 4-3: Material Properties 2 [61, 62]

4.3 Tests

After printing the Hinges, tests were conducted. First, every Hinge was visually examined for printing failures and its accuracy, and its state was documented using pictures. Fig. 4–9 shows a draft of the test execution.

One comparison characteristic is the “Sag by its Own Weight” angle (SOW-angle), which indicates the stiffness of the Hinge and should ideally be 0° . When one rod of the Hinge is held horizontally, the angle between the horizon and the other rod is the SOW-angle. Since the SOW-angle is dependent on the rod weight, it can only be compared within each test group (same rod material and volume). The SOW-angle is 0° , if not mentioned otherwise.

For the test, the Hinge was bent by 180° (“Displacement-angle” between 1 and 2 in Fig. 4–9), so that the bending radius is nearly 0° , and held in place for one minute. Here, the rods execute a “Reopening-force”, which is dependent on the Displacement-angle.

Then, the upper rod was held horizontally, while the lower rod was released. The lower rod quickly snapped back to a specific angle (called the “Quick Reopening-angle”) and slowly moved further to the final “Reopening-angle” (between 2 and 3 in Fig. 4–9), which was measured with a protractor. If the reopening stopped at the SOW-angle, the Hinge was turned to remove the influence of gravity. Then the state of the Hinges was documented with pictures again.

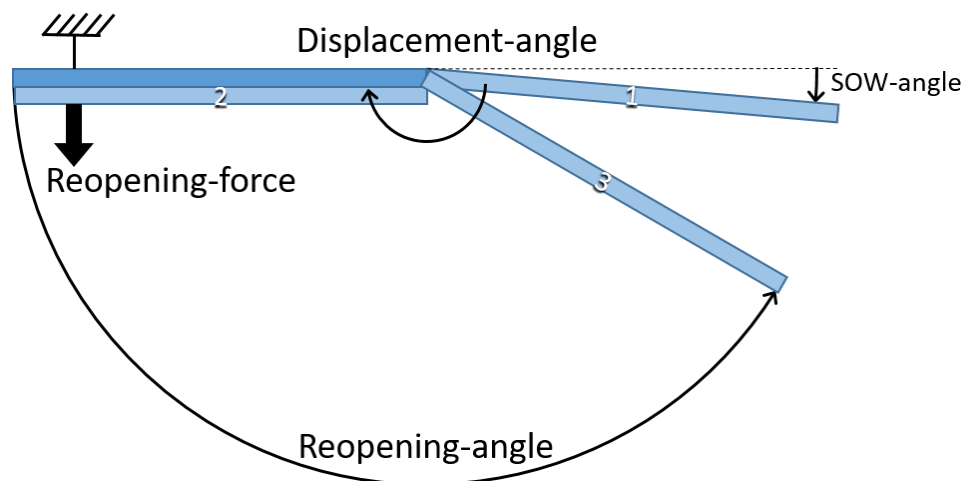


Fig. 4–9: Test Execution Draft

For the first prints, the typical FDM materials Polylactide (PLA), Tough PLA, Acrylnitril-Butadien-Styrol (ABS) and Polyethylenterephthalat + Glykol (PETG) have been used, but no design could be fully deployed. Therefore the material Flex has been used and the deployment worked well for all designs. The softness of the Hinges, which are also a part of the stiffening structure, was a problem. This leads to the idea of using such a flexible material only at specific points of the Hinge, or to make a mixture of flexible and hard materials. The examination of these ideas is described in Chapter 4.3.3.

4.3.1 Form 2

The Form 2 printer has a higher precision than the FDM printers. However, parts smaller than approximately 1 mm in diameter become too brittle, and separating very flat prints from the platform leads to a permanent curvature of the print.

High Temp material is too brittle for all designs.

Tough material has a Reopening-angle of 100° to 150° and breaks after a few foldings.

Durable material has Reopening-angles of 90° for the Torsion-Hinge and rod, 80° to 100° for the O-Hinge and 100° to 130° for the Oval-Hinge. This means that plastic deformation happens in every design, just a little less than in the rod. Elongation of 49% is not enough for these designs, but it could be sufficient for a Torsion-Hinge with longer Torsion-Rods (adaptability of the Torsion-Hinge to material properties is one of its advantages). Tests showed a Reopening-angle of 125° to 150° for the long Torsion-Hinge. Fig. 4–10 shows a picture of Torsion-Hinges made out of "Durable" material before the test.

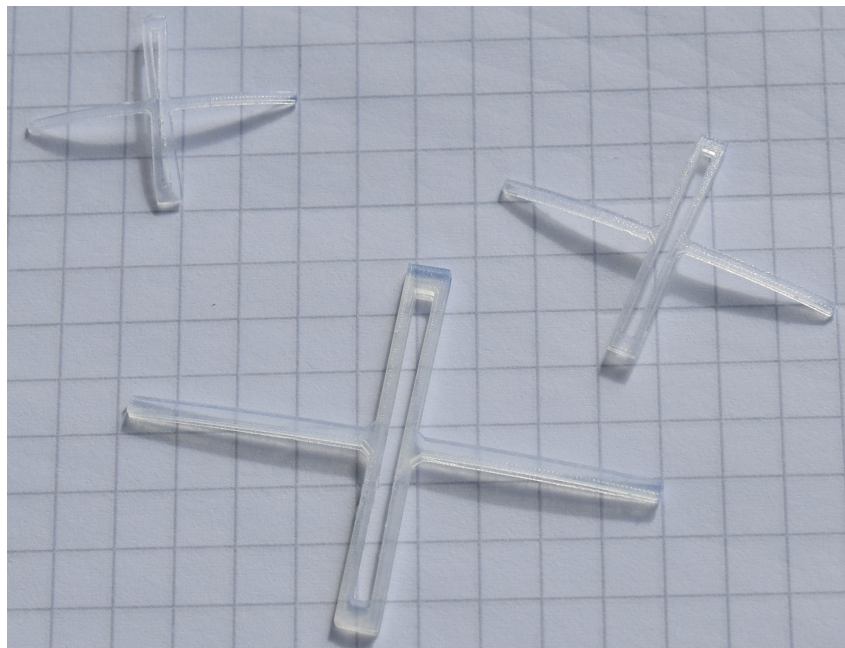


Fig. 4–10: Printed Hinges, Durable

Flexible material leads to a Reopening-angle of 180° for every design, but has a low Reopening-force. Repeated actuations did not change the result, except in the O-Hinges, which eventually breaks in the middle. Just like the Flex material of the Prusa printer, the reopening works perfectly, but it has a low Reopening-force and general stability.

4.3.2 Mark Two

The Mark Two printer can insert fibers while printing, but for this, the print has to be large enough. The printed O-Hinge (made of Nylon and High Strength High Temperature Fiberglass) had a 6 mm * 3 mm cross section area of the rod, so that two fibers were able to lay beside each other. Since this printed O-Hinge is significantly larger than the other prints, the test results are hard to compare. However, the Reopening-angle was 140° (125° quick Reopening-angle). This difference in when the Reopening-angle is reached indicates the Reopening-force. The 125° angle was reached nearly immediately and therefore, the Reopening-force was large. From 125° to 140° the reopening was slow with a small Reopening-force.

Fiber insertions are more useful as reinforcement of the structure than in the Hinges, but only if they can be smaller than the ones made with the Mark Two printer. Since this can not be tested with the available means, it is not studied further at this point.

Onyx material was used for prints of 1 mm to 2 mm rod height and were not precise enough. They had a Reopening-angle of 100° for the O-Hinge and 125° for the Torsion-Hinge. The material is neither brittle nor flexible, but has a large plastic deformation region.

Nylon material has a Reopening-angle of 110° for a rod with 2 mm height. An O-Hinge with 1.7 mm rod height reopens to an angle of 165° (150° quick). Fig. 4–11 shows these two Hinges after the tests were conducted, as well as a normal Torsion-Hinge (1.2 mm height) that only had a Reopening-angle of 140°. This result is outperformed by the long Torsion-Hinge (1.5 mm rod height), which had a Reopening-angle of 170° (160° quick). This proves the adaptability of the Torsion-Hinge to material properties. The permanent deformations are explained by the big difference between Elongation at Yield (27%) and Elongation at Break (260%).

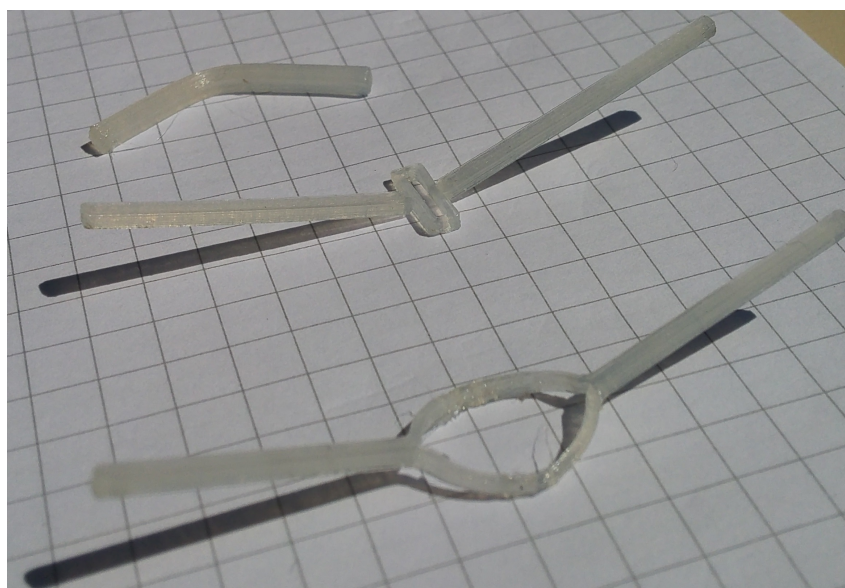


Fig. 4–11: Printed Hinges, Nylon

4.3.3 Objet260 Connex3

The Objet260 Connex3 printer uses the MJM method and therefore can mix two different materials. In the following tests, a stiff material RGD525 or VeroBlue is used for the rods and a mixture of the stiff and the flexible material (TangoBlack+ or Agilus30 Black) is used for the Hinges. The material properties of these mixtures are listed in Tab. 4–3.

Fig. 4–12 shows Hinges printed with the Objet260 printer. The Hinges are, from left to right: Parabola-, O2-, O2-, Bowl-, Big-Hole-, Rod, Rod, Rod. All rods are white (RGD525), while the flexible part has different gray shades, which indicates its mixture (white RGD525 and black TangoBlack+).

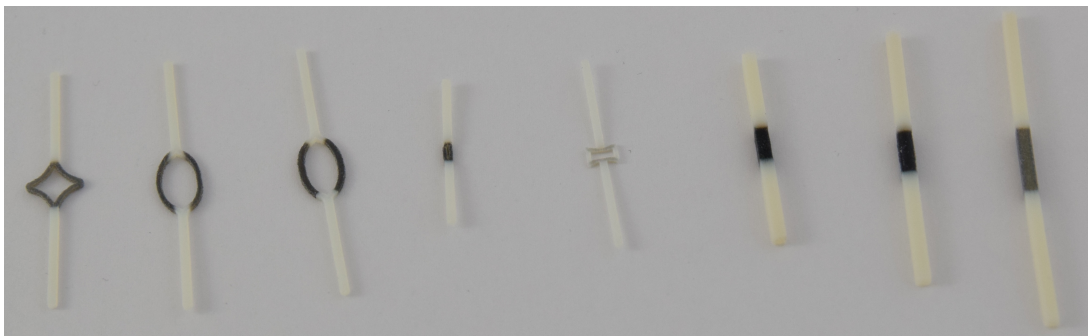


Fig. 4–12: Printed Hinges, Objet260

The objective is to find the best material mixture for every Hinge design and to compare the results of the Hinge designs with each other.

Rod

A rod (4 mm² cross section area) with a long section (10mm) of RGD5250 got ripped when bent by 20° Displacement-angle, while having a SOW-angle of 0°. The more flexible material FLX9670 has a SOW-angle of 4° and a Reopening-angle of 170°. When the section of FLX9670 material is reduced to 6.3 mm or 5 mm, the SOW-angle is 0°, but the material rips on the stretched side. An even more flexible material, FLX9640, in a 6.3 mm section has a SOW-angle of 5° to 10° and a Reopening-angle of 175°.

Even though good Reopening-angles can be reached, there is little room for improvement and the SOW-angle was not 0°, which means the rod is too soft.

Bowl-Hinge

The Bowl-Hinge printed with RGD5250 was too stiff. The walls pressed towards outside and broke early into the bending. However even without the walls it had a Reopening-angle of 160° (90° quick). For the next test (with a 1 mm² rod cross section area), the walls were thicker and the material was more flexible, but the walls of the print with FLX9685 broke again. The Reopening-angle was 170° (140° quick). With FLX9660, the walls stayed intact and the quick Reopening-angle was 180°.

Since the SOW-angle for all tests was 0°, the material FLX9660 leads to good overall test results for the Bowl-Hinge.

Parabola-Hinge

The Parabola-Hinge combines bending and torsion, like the Oval-Hinge, but in a different order. The bending takes place close to the rod and torsion occurs at the sides.

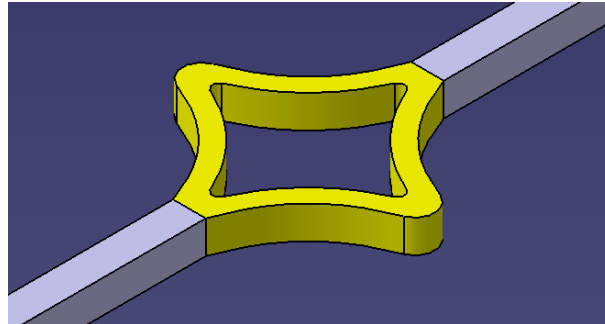


Fig. 4–13: Design: Parabola-Hinge

The first print of the Parabola-Hinge with RGD5215 was too hard and broke at the first bending. The second print with RGD525 had a Reopening-angle of 160° (110° quick) (see Tab. 4–4) and broke after a few actuations. It also showed that the torsion was not evenly distributed due to thickness changes. The design was improved to the one shown in Fig. 4–13, but the disadvantage of a complicated design and flux of force remains.

The improved design was printed with 1 mm² rod cross section area and four different material mixtures:

Material	SOW-angle	Reopening-angle
RGD5225	0°	Breaks when bent by 100°
RGD5250	0°	140° (90° quick)
FLX9685	13°	175° (150° quick)
FLX9670	20°	170° (145° quick)

Tab. 4–4: Test Results Parabola-Hinge

Even though FLX9685 reaches a good Reopening-angle, it has a large SOW-angle and is therefore very soft. Because of these unpromising test results and the complicated design and flux of force, the Parabola-Hinge is not listed among the best final designs in Chapter 4.1 and is not studied further at this point.

O4-Hinge

The O4-Hinge has four small sections with flexible material as shown in Fig. 4–14. The tests showed that the flexible section at the base of the O4-Hinge barely changed when the Hinge was bent. All the bending was done in the central flexible section that ripped apart, even though very flexible materials, FLX9660 and FLX9640, were used.

Therefore, the design was improved to make the base section more rigid and the central section larger, resulting in the O2-Hinge.

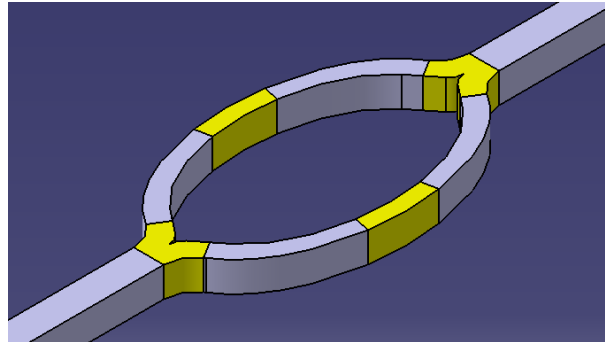


Fig. 4–14: Design: O4-Hinge

O2-Hinge

This improved design was printed with RGD5250, but the connection between stiff and flexible sections broke apart when bent. The design was improved by changing the angle of this connection to enlarge the area (compare Fig. 4–7 with Fig. 4–14). Tests with this design are marked with (1) in Tab. 4–5 and showed better results than the old connection. The test (2) was reduced 25% in size, so that the rod edge length was 0.75 mm instead of 1 mm for all other tests.

	Material	SOW-angle	Reopening-angle	Note
	FLX9695	0°	165° (135° quick)	to stiff, nearly brakes
(1)	FLX9695	0°	170° (130° quick)	to stiff, nearly brakes
	FLX9685		170° (150° quick)	
(1)	FLX9670	10°	175° (165° quick)	
(2)	FLX9660		170° (150° quick)	
	FLX9650	17°	170° (160° quick)	

Tab. 4–5: Test Results O2-Hinge

The test results show an optimum Reopening-angle (175°) for FLX9670, which has a large SOW-angle (10°). However, similar materials have a nearly identical Reopening-angle (170°), which makes the optimum for FLX9670 less important.

In general, the test results were positive and the O2-Hinge can be optimized by FEM analysis.

Filled-O-Hinge

For the first tests, pure Agilus30 Black was used for the flexible part. This led to a SOW-angle of 10° (one specimen had 15° in one direction and 5° in the other, so the print was not symmetrical) and a Reopening-angle of 180° , but with a small Reopening-force. Bending the Hinge in slightly different ways led to the same results, which means that it is robust.

The following tests with FLX97-40, -50, -60, -70 and -85 did not show much difference among each other. FLX9785 had a SOW-angle of 0° , while the others had 4° . The Reopening-angle was between 163° and 172° , while the quick Reopening-angle was around 157° , which indicates a stronger Reopening-force than for most of the other tests.

A test with a flatter flexible part of the Hinge, like the “Wide and Flat” design, significantly reduces the stiffness in the direction of deployment/folding (SOW-angle of 25°).

Oval-Hinge

The test results for the Oval-Hinge listed in Tab. 4–6 show a large SOW-angle, but low Reopening-angles. However, using a harder material leads to breaking. An optimization by FEM analysis between material characteristics and design is necessary to make this Hinge design useable.

Material	SOW-angle	Reopening-angle
RGD K60		Breaks within the flexible section
FLX9795	10°	145° (100° quick)
FLX9785	15°	145° (100° quick)
FLX9770	25°	135° (110° quick)
FLX9760	30°	135° (120° quick)

Tab. 4–6: Test Results Oval-Hinge

Torsion-Hinge

These first tests have been conducted with an early design of the Torsion-Hinge, called the “BigHole”-Hinge shown in Fig. 4–15.

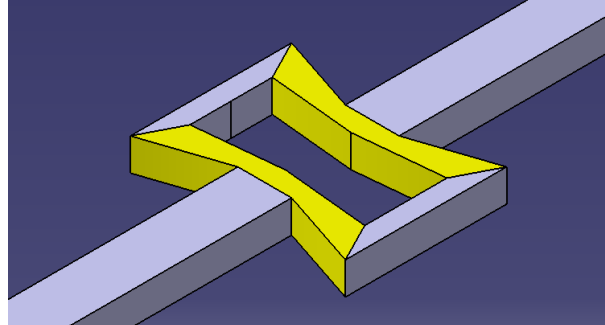


Fig. 4–15: Design: BigHole-Hinge

Material	SOW-angle	Reopening-angle
RGD5225	0°	Breaks within the flexible section
RGD5250	0°	165° (145° quick)
FLX9695	0°	135° (100° quick)
FLX9660	15°	175° (160° quick)

Tab. 4–7: Test Results BigHole-Hinge

The small Reopening-angle for FLX9695 is noticeable, which could be caused by a faulty specimen (The print could not be repeated due to timing issues.). FLX9660 is too soft (SOW-angle of 15°), but RGD5250 has a good Reopening-angle. This shows that the Torsion-Hinge is applicable for stiffer materials.

Next, the Torsion-Hinges, described in Chapter 4.1.2, have been tested. The short version had Torsion-Rods with a cross section of 0.75 * 0.6 mm and a width of 4.5 mm. Tab. 4–8 shows the test results. The SOW-angle is large and increases with flexibility. The Reopening-angle is around 140° and 150° for the stiffest material FLX9785. Since all the chosen materials had a large SOW-angle, every material was too flexible for good test results.

Material	SOW-angle	Reopening-angle
FLX9785	10/30°	150° (130° quick)
FLX9770	20°	140° (120° quick)
FLX9760	20/30°	135° (130° quick)
FLX9750	30°	140° (130° quick)

Tab. 4–8: Test Results short Torsion-Hinge

The long version had Torsion-Rods with a cross section of $0.45 * 0.6$ mm and a width of 21 mm. Even though the tests were done with stiffer materials, the SOW-angles were large ($22-35^\circ$) and the Reopening-angle was small (130°). However, the stiffest material RGD K60 had the best test results with a SOW-angle of 0° in one and 15° in the other direction. The Reopening-angle was 160° . An even stiffer material would probably lead to better results.

Noticeable during manufacturing is that the Torsion-Rods were wavy, mainly due to the excavation process. Further tests of the specimen from this printer and material should be conducted with a minimum cross section of $1 * 1$ mm for the Torsion-Rods, which increases the repeatability of the test results.

Material	SOW-angle	Reopening-angle
RGD K60	$0/15^\circ$	160° (120° quick)
RGD K50	22°	130° (110° quick)
FLX9785	35°	130° (130° quick)

Tab. 4–9: Test Results long Torsion-Hinge

4.4 Comparison and Selection

The objective is to compare the results of the Hinge designs among each other and to find the best material for the Hinge design. This will be the basis for a FEM analysis. The main properties to compare are the Reopening-angle and the stiffness (indicated by the SOW-angle)

Tests with pure flexible material showed that every Hinge can deploy by 180° , but has a large SOW-angle. Since the Hinge is also part of the stiffening structure, the stability is not sufficient when using pure flexible material.

The Hinges with the best Reopening-angles and a low SOW-angle are:

Bowl-Hinge: The SOW-angle for all tests was 0° and the material FLX9660 (Tensile Strength 2.8-4 MPa, Elongation 60-80%) had a Reopening-angle of 180° . The 3D printed Bowl-Hinge can be optimized and converge with the Tape-Spring-Hinge design. However, the design is limited by its thin walls. They are prone to rips and limit the down-scalability of the design. Therefore it is not applicable for the Rip-Stop structure.

O2-Hinge: The tests found a Reopening-angle of 170° with a SOW-angle of 0° for the materials FLX9695 and FLX9685. These materials have a Tensile Strength of 6 to 12 MPa and Elongation at Break of 27% to 50 %.

Filled-O-Hinge: The chosen material had small influence on the good test results (Reopening-angle of 170° and SOW-angle below 5°). The Hinge is robust, has a larger Reopening-force, but also a bigger mass than the other Hinges. In a FEM Analysis, the O2- and Filled-O-Hinge, as well as the Oval- and Stretched-O-Hinge, can use the same model for their shapes, when they have an inner and outer primary and secondary diameters (Inner Diameters are zero for the Filled-O-Hinge).

Torsion-Hinge: The test results show that the Torsion-Hinge is the best choice when using stiff materials (RGD5250 lead to 0° SOW-angle and 165° Reopening-angle). The easy adjustability of the Torsion-Rod length to accommodate a certain material is a big advantage, when it comes to manufacturing a space qualified Hinge. The number of available materials with fitting characteristics will be limited, for example, due to outgassing and thermal requirements. For now, the studies assume the simplification that all material characteristics can be manufactured in a space qualified way. When the desired material characteristics are known, a manufacturable, space qualified material with close characteristics has to be found. Then, the design of the Hinge (and possibly of the stiffening structure) has to be adapted to accommodate that material.

Additionally, the geometry of the Torsion-Hinge is simpler than the O2-/Filled-O-Hinge and therefore, it is a better starting point.

The Torsion-Hinge is selected for a FEM analysis and optimization.

5 Finite Element Analysis

The objective of the FEA is to improve the geometry of the Torsion-Hinge, to show that the general Hinge-concept works as intended. The Hinge will be tested, according to the analysis, to validate the model and analysis.

This will then form the basis for the development of the final Hinge, which will be done, when more requirements (Membrane, Material, Printer, Stiffness) are defined.

Parametrisation

The model and analysis is done within the Ansys Parametric Design Language (APDL), using only commands to form a script that can be repeated easily. The geometric shape of the Hinge is fixed (and has to be adapted for the O-Hinges, while the rest of the script can stay the same), but the dimensions are defined by parameters. A python script changes these parameters, reruns the analysis and saves the results in a table for comparison. This way, instead of a value, a range can be specified for every dimension, to find the wanted (e.g. in regards to stiffness and size) or optimal solution within these ranges. This saves time and could lead to new resulting Hinge designs.

5.1 Model

In this chapter, the FEM model and analysis (and possible variations) are briefly described. This is followed by the results of the analysis in the next section.

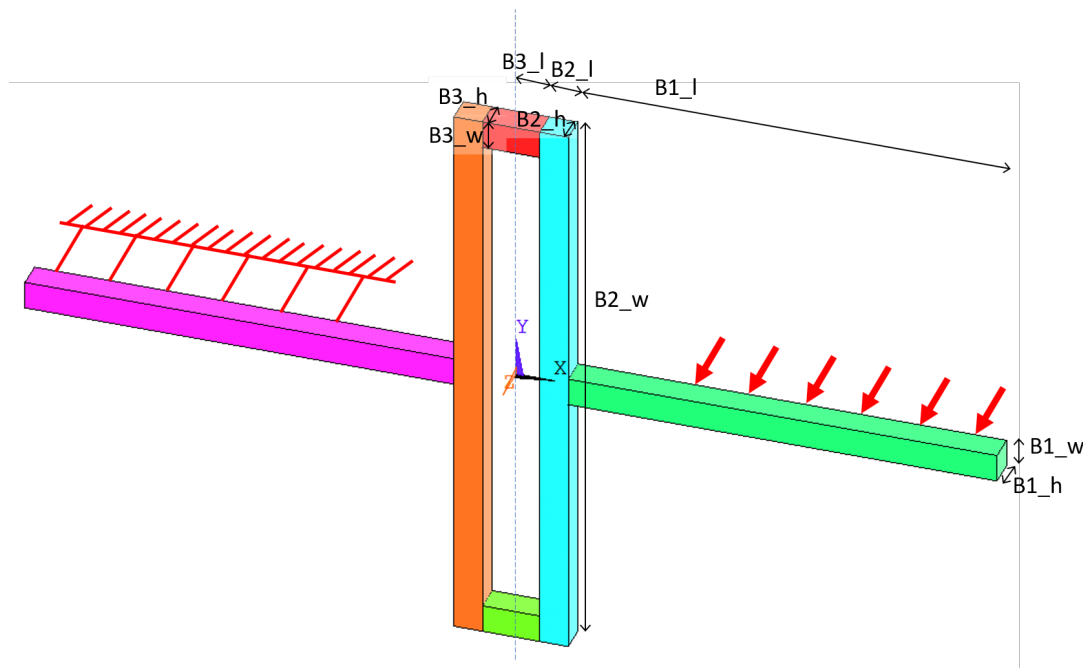


Fig. 5–1: Parameters of the Torsion-Hinge Model

5.1.1 Input

The Torsion Hinge geometry is made out of 6 Blocks as shown in Fig. 5–1, with their relating parameter names. The most influential parameter is B2_w, followed by B2_l and B2_h and the material of Block 2 (Torsion-Rod).

Material

Every Block can be assigned a different material, but for a validation test at the DLR facilities, a present 3D printer should be used. Considering the test results from the previous chapter, the material selection is limited to:

- Nylon
- Durable
- Material mixtures of the Objet260 Connex3 printer

However, the datasheets for Objet260 materials do not provide information on the Young's modulus, which is the most important characteristic for the FEM model. Therefore, the whole part will be made out of only one material: Nylon or Durable.

The Durable material datasheet does not provide information about the Yield Stress. Therefore, the “Flexural Stress at 5% Strain” value will be used. For Nylon, the analysis has to be done with Tensile values, because no value for “Flexural Stress at Yield” is given in the datasheet (see Tab. 4–2).

Boundary Conditions and Loads

The left rod (purple in Fig. 5–1) is fixed on the far side ($-z_{max}$), except for the 5 mm closest to the Torsion-Rod (orange in Fig. 5–1).

On the same area on the right rod, a perpendicular pressure is applied to the surface area. This means it is not acting towards the +z direction all the time, but moves with the displacement of the rod. This pressure results in a displacement of the right rod bending towards the left rod. This leads to a resulting angle between the two rods (e.g. Reopening-angle = 10° , which means the right rod is displaced by 170°). The pressure is called the Reopening-force at that specific angle.

Gravity is applied in -z direction.

After this information is given to the model, a mesh is created and the model is solved iteratively (because of large-deflection effects). A mesh is shown in Appendix A.1.

5.1.2 Output

The input parameters that the python script gives to the analysis were listed above. Here, the output of the analysis is described. Because of many reruns of the analysis with different parameters, the output has to be reduced to the most important values, which should be easy to compare among each result. They are listed here:

- **The Maximum von Mises Stress**

It has to be below the yield stress value, because otherwise permanent plastic deformation takes place. The analysis is conducted to avoid this.

- **Reopening-force (XZ-plane) from 180° to 0°**
Could be a few exemplary points (e.g. at 180° and 10°) instead of a graph.
- **Picture of the stress distribution in the Hinge at 180°**
- **Stability regarding every plane at 0°**
For example: What force is needed to displace the rod by 1° in every plane (XY, YZ, XZ).
- **Volume and Mass**

5.1.3 Variations

The FEM model and analysis used for design improvement are subject to change in the development process. The most important variations are listed here.

Linear Material Behaviour:

The linear material model is valid only within the elastic deformation region. If the von Mises stress is higher than the yield stress of the material, permanent plastic deformation takes place and it will not reopen at 180°. Therefore the result is a failure and the accuracy does not matter. Furthermore the data sheets of relevant 3D printing materials do not provide sufficient information for the nonlinear material model. If the nonlinear model will be implemented at a later point for a better accuracy at the transition from elastic to plastic deformation, the necessary material characteristics have to be determined first.

Material characteristics:

The Young's modulus and the density are taken from the datasheet, while the Poisson's ratio is a mean value for plastics, and therefore, unprecise. However, the Poisson's ratio has very little effect on the results.

The strength of the bond between different materials (depending on the printer and materials) or between the Hinge and the membrane has to be identified by experiments.

Contact of Surfaces

In the analysis, a displacement can make a block move inside another. To avoid this, contact conditions can be added. Although this significantly increases the computing time. Therefore, it is done only for a detailed analysis and not for the parametrisation.

Symmetry:

YZ-Plane: The load is not symmetric to this plane. The Torsion-Rod-Connection can not be a fixed support, because it has to be able to move in Y- and Z-direction or turn around their X-axes. Nor can a symmetric condition be applied here, because then, a different fixed support against Y- and Z-displacement is needed, but does not exist.

XY-Plane: The load is not symmetric to this plane.

XZ-Plane: Possible, but the model geometry is not using symmetry yet. At a later point, before the large-scale parametrisation is conducted, the symmetry regarding the XZ-plane should be applied.

Membrane:

The membrane will not be considered for the validation test, but is necessary for the final design. A geometric “Shell” has to be added to the model for this.

Geometry:

These possible changes of the model geometry will not be examined in this thesis:

- Different cross section profiles
- Changes of cross section dimensions within one block
- Rounding of the edges (Test showed they have little influence on the stress, but additional parameters increase the calculation time.)
- Different transition from material 1 to material 2 (The strength of this bond is not considered in the analysis.)

5.2 Analysis Results

For the first FEA, the used material (Nylon and Durable) and the rod cross section were set (1.5 mm * 1.5 mm or 2 mm * 2 mm). The Reopening-force was iteratively changed to lead to a Displacement-angle of approximately 180°. The deviation between 180° and the actual Displacement-angle is explained by the inaccuracy of missing contact conditions.

To lower the Maximum von Mises Stress and increase the Reopening-force at that 180° angle, the other parameters were adapted. Some resulting Hinge geometries are exemplified here and tested in the next chapter.

The Output described in Chapter 5.1.2 is reduced here, because stability, volume and mass are detailed performance criteria, while the objective here is a proof of concept.

5.2.1 Durable

The input parameters of the Torsion-Hinge, called “B2_w-47 Durable”, are listed in Tab. 5–1.

The stress distribution of this analysis is shown in Fig. 5–2:

- The left Hinge has a Reopening-force of 10 kN/m² at a Displacement-angle of 66° and a Maximum von Mises Stress of 10.3 MPa.
- The next Hinge from the left has a Reopening-force of 15 kN/m² at a Displacement-angle of 96° and a Maximum von Mises Stress of 14.4 MPa.
- The third Hinge from the left has a Reopening-force of 25 kN/m² at a Displacement-angle of 140° and a Maximum von Mises Stress of 22 MPa.
- The right Hinge has a Reopening-force of 35 kN/m² at a Displacement-angle of 184° and a Maximum von Mises Stress of 27.4 MPa.

The color scale in Fig. 5–2 is only valid for the right Hinge. The other Hinges have their Maximum von Mises Stress written below the picture. For the right Hinge, the Maximum von Mises Stress is slightly larger than the yield stress, but this result was accepted, because Fig. 5–2 shows, that there is very little area where the stress is higher than

Parameter	Value	Unit
B1_h	1.5	mm
B1_l	15	mm
B1_l	1.5	mm
B2_h	1.5	mm
B2_l	0.7	mm
B2_w	47	mm
B3_h	1.5	mm
B3_l	1	mm
B3_w	0.7	mm
Mat_Density	1000	kg/m ³
Mat_Young's modulus	820	MPa
Mat_Poisson's ratio	0.39	
Mat_Yield stress	27.2	MPa
Mesh Size	0.0004	m
Reopening-force	35	kN/m ²

Tab. 5–1: Input Parameters of the B2_w-47 Durable Torsion-Hinge

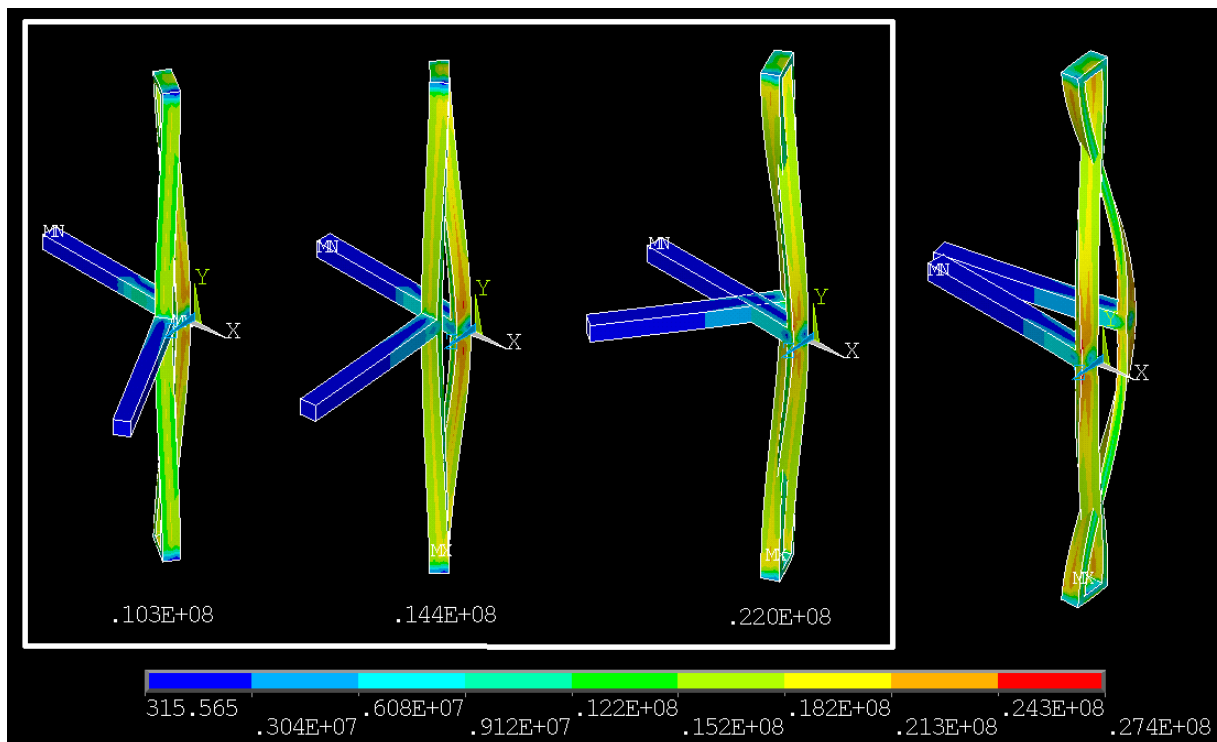


Fig. 5–2: B2_w47 Durable

27.2 MPa, and this Hinge has one of the lowest Maximum von Mises Stress reached in the analyses for Durable material. Even though the final position of the Hinge is impossible, because parts are within each other, the results are accurate enough for an improvement of the design from the previous chapter.

5.2.2 Nylon

The input parameters of the Torsion-Hinge, called “B2_w-45 Nylon”, are listed in Tab. 5–2.

The stress distribution of this analysis is shown in Fig. 5–3:

- The left Hinge has a Reopening-force of 10 kN/m² and a Maximum von Mises Stress of 12.8 MPa at a Displacement-angle of 61°.
- The middle Hinge has a Reopening-force of 20 kN/m² and a Maximum von Mises Stress of 22.9 MPa at a Displacement-angle of 114°.
- The right Hinge has a Reopening-force of 33 kN/m² and a Maximum von Mises Stress of 32.6 MPa at a Displacement-angle of 169°.

The color scale in Fig. 5–3 is only valid for the right Hinge. The other Hinges have their Maximum von Mises Stress written below the picture. For the right Hinge, the Maximum von Mises Stress is slightly larger than the yield stress, but this result was accepted, because this Hinge has one of the lowest Maximum von Mises Stresses reached in analyses for Nylon material. Even though the final position of the Hinge is impossible, because parts are within each other, the results are accurate enough for an improvement of the design from the previous chapter.

Parameter	Value	Unit
B1_h	2	mm
B1_l	20	mm
B1_l	2	mm
B2_h	2	mm
B2_l	0.8	mm
B2_w	45	mm
B3_h	2	mm
B3_l	1	mm
B3_w	0.8	mm
Mat_Density	1100	kg/m ³
Mat_Young's modulus	940	MPa
Mat_Poisson's ratio	0.4	
Mat_Yield stress	31	MPa
Mesh Size	0.0004	m
Reopening-force	33	kN/m ²

Tab. 5–2: Input Parameters of the B2_w-45 Nylon Torsion-Hinge

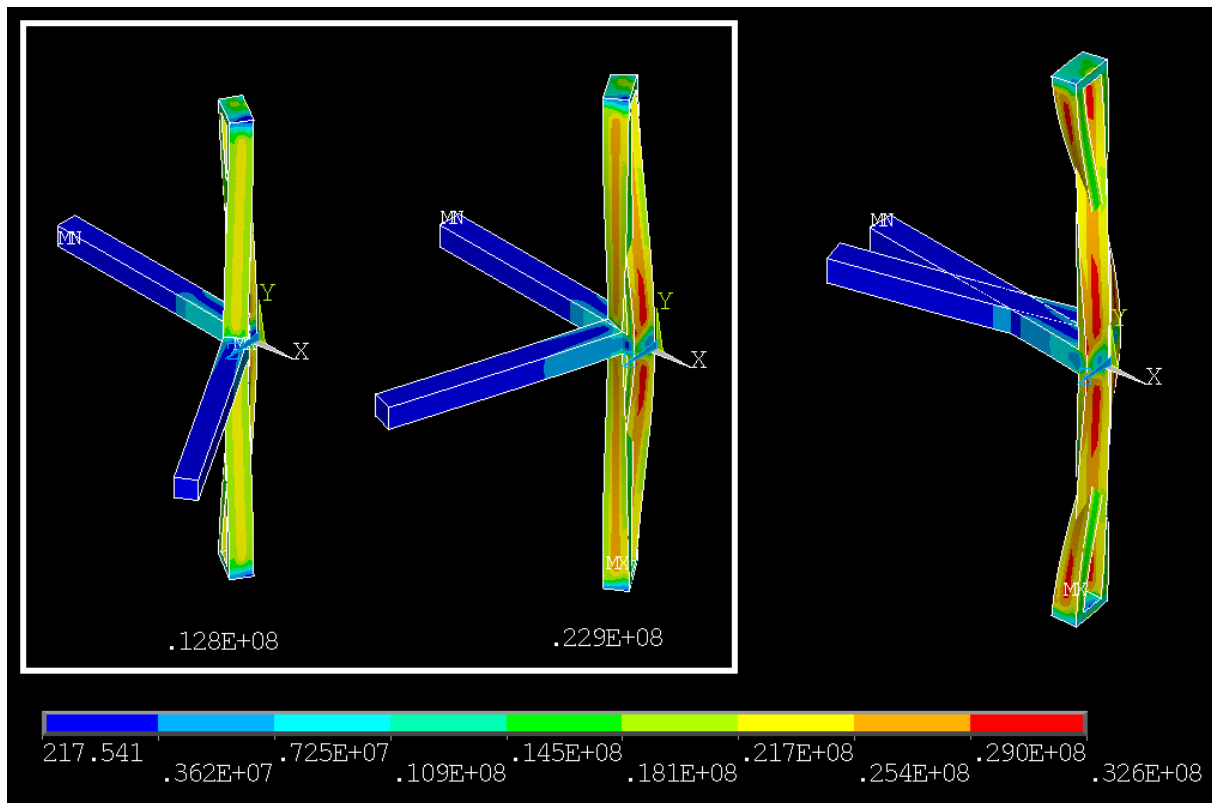


Fig. 5–3: B2_w45 Nylon

5.2.3 2TR-Hinge

One finding of the analyses is that (beside B2_w) a thin Torsion-Rod (B2_l) strongly decreases the von Mises stress. However, this goes along with a significant reduction of stability and Reopening-force. To counteract this, multiple thin Torsion-Rods can be used.

Analyses were conducted with two thin Torsion-Rods that were very close to each other, and the resulting design is called the 2TR-Hinge (2 Torsion-Rods Hinge) and is shown in Fig. 5–4. Even more Torsion-Rods are possible, but they increase the bending radius of the Hinge, and are therefore, not examined.

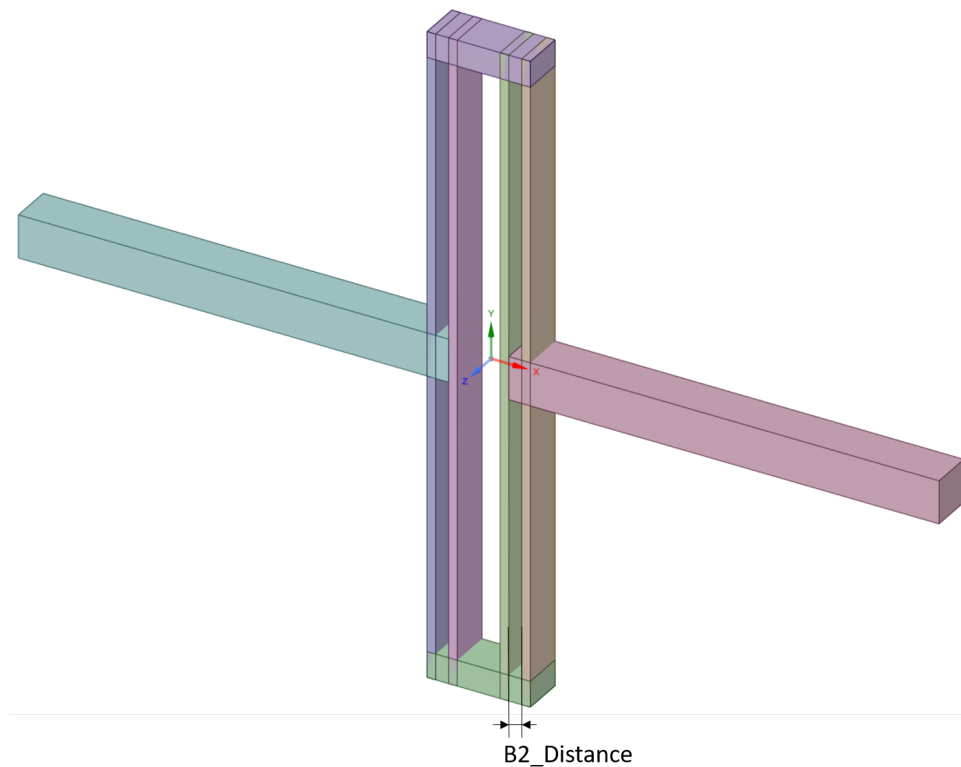


Fig. 5–4: CAD Image of a 2TR-Hinge

The input parameters of the Torsion-Hinge, called “2TR B2_w-45 Nylon”, are listed in Tab. 5–3.

The stress distribution of this analysis is shown in Fig. 5–5:

- The left Hinge has a Reopening-force of 35 kN/m^2 and a Maximum von Mises Stress of 21.7 MPa at a Displacement-angle of 98° .
- The middle Hinge has a Reopening-force of 60 kN/m^2 and a Maximum von Mises Stress of 33.3 MPa at a Displacement-angle of 150° .
- The right Hinge has a Reopening-force of 70 kN/m^2 and a Maximum von Mises Stress of 35.9 MPa at a Displacement-angle of 169° .

The color scale in Fig. 5–5 is only valid for the right Hinge. The other Hinges have their Maximum von Mises Stress written below the picture. For the right Hinge, the Maximum von Mises Stress is larger than the yield stress, but this analysis was conducted with similar sizes, to show its difference from the B2_w-45 Nylon Hinge. Only B3_w (insignificant) and the Number of Torsion-Rods changed. The Maximum von Mises Stress is 3.3 MPa (10 %) larger, but the Reopening-force has doubled to 70 kN/m^2 .

More Hinges were analyzed and their parameters and output is listed in Appendix A.2. A short overview of all analyzed Hinges is given in Tab. 5–4, Tab. 5–5 and Tab. 5–6

Parameter	Value	Unit
B1_h	2	mm
B1_l	20	mm
B1_l	2	mm
B2_h	2	mm
B2_l	0.8	mm
B2_w	45	mm
B2_Distance	0.3	mm
B3_h	2	mm
B3_l	1	mm
B3_w	1.2	mm
Mat_Density	1100	kg/m ³
Mat_Young's modulus	940	MPa
Mat_Poisson's ratio	0.4	
Mat_Yield stress	31	MPa
Mesh Size	0.0004	m
Reopening-force	70	kN/m ²

Tab. 5-3: Input Parameters of the 2TR B2_w-45 Nylon Hinge

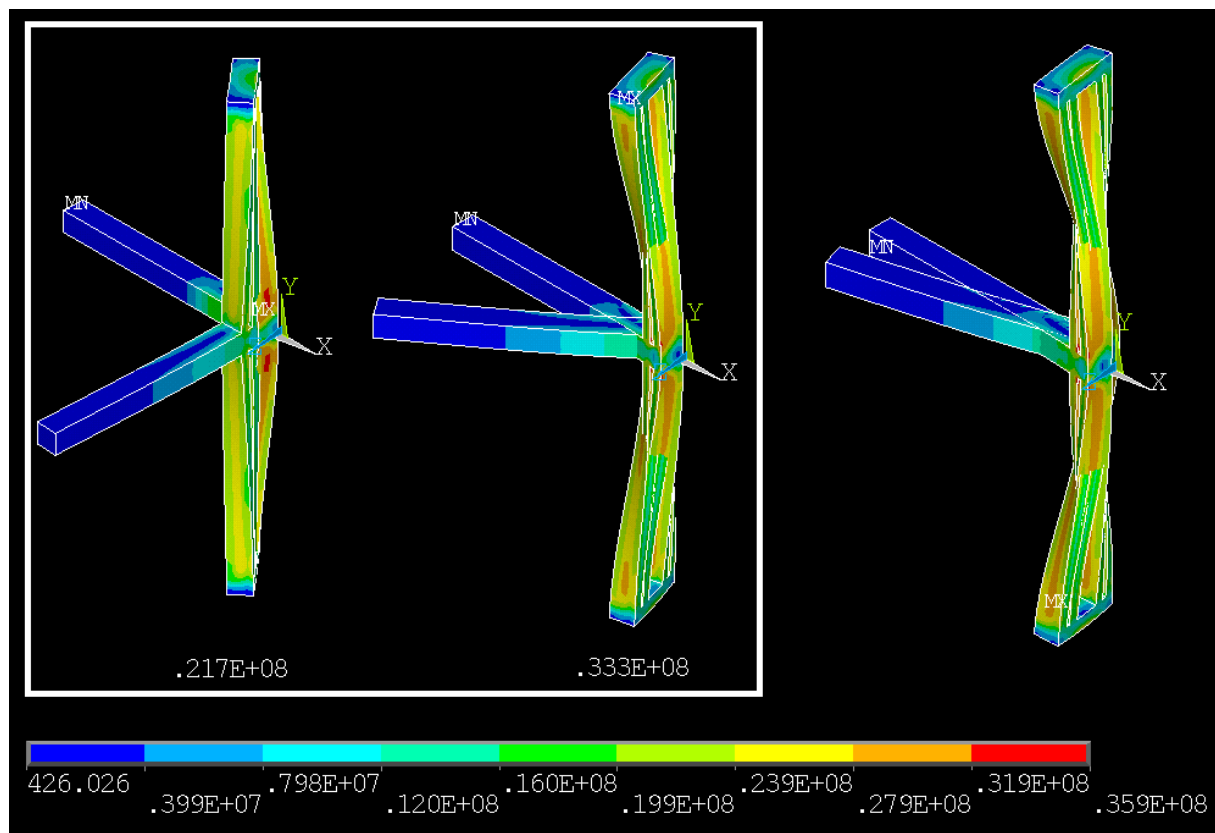


Fig. 5-5: 2TR B2_w45 Nylon

5.3 Test Results and Comparison with FEA

The FEA was used to improve the Torsion-Hinge design, by increasing the Reopening-force and lowering the Maximum von Mises Stress - which is expected to increase the Reopening-angle. The Reopening-angle, which is the most important characteristic, can not be provided by the analysis.

Tests were conducted to check the expectation about a correlation between the Reopening-angle and the Maximum von Mises Stress, and to prove the basic Torsion-Hinge concept.

The previously identified Hinge parameters were printed and tested in the same way as described in Chapter 4.3. The resulting Reopening-angle is listed in this chapter, alongside the analysis results for every Hinge.

The SOW-angle was 0° for every test and is therefore no longer mentioned.

5.3.1 Durable

The results are shown in Tab. 5–4.

The reopening happened slowly to a Reopening-angle of 150° for the “B2_w-47 Durable” Hinge. After lying on a table for an hour (gravity was supporting the reopening movement) the Hinge reopened fully (180°).

The same behaviour was observed for a “B2_w-37 Durable” Hinge (parameters described in Appendix A.2), but with a Reopening-angle of 140°.

Name	Test Results	Analysis Results	
	Reopening-angle	Maximum von Mises Stress	Reopening-force
B2_w-37 Durable	140° (30° quick)	27.2 MPa	30 kN/m ²
B2_w-47 Durable	150° (30° quick)	27.4 MPa	35 kN/m ²

Tab. 5–4: Test and Analysis Results Durable Hinges

The Durable “Flexural Strength at 5% Strain” is 27.2 MPa. Because of the lack of a Yield Stress value in the datasheet, this was taken as the Yield Stress. But now, the results indicate that their 5% strain is outside of the elastic deformation region and leads to the poor Reopening-angle.

Durable material takes much more time to reopen, which indicates a small Reopening-force in that area. The Reopening-angle stayed in the same region as in the previous tests (see 4.3.1).

Even though the Form 2 printer is very precise, small rods used in the Hinges, have curvatures after separating them from the platform. This leads to unprecise parts that differ from the analysis. Therefore, Durable is a poor material for the validation test.

5.3.2 Nylon

The Hinges were designed with a minimum wall thickness of 0.4 mm, because that is the Nozzle diameter of the Mark Two printer.

However, it turned out that the printer can not print that finely and therefore automatically makes small parts thicker, so that they are printable. For these cases, the geometry parameters listed in the Appendix differ between “wanted” and “printed” values. The analysis showed a good result for the “wanted” value, however, the “printed” value was printed and tests had to be conducted with this Hinge.

Then a new analysis for the printed geometry was conducted, which is why the Maximum von Mises Stress is larger than the Yield Stress. Since this makes the analysis results inaccurate, the Maximum von Mises Stress values are larger than the 54 MPa Tensile Strength from the material properties in Tab. 4–2, even though no Hinge broke.

The geometry and detailed analysis results of the Hinges are listed in Appendix A.2. The test results are shown in Tab. 5–5.

Name	Test Results	Analysis Results	
	Reopening-angle	Maximum von Mises Stress	Reopening-force
B2_w-40 Nylon 1	170° (150° quick)	151.3 MPa	100kN/m ²
B2_w-40 Nylon 2	165° (150° quick)	79.9 MPa	55 kN/m ²
B2_w-45 Nylon	170° (150° quick)	32.6 MPa	33 kN/m ²
B2_w-46 Nylon 1	175° (150° quick)	44.6 MPa	55 kN/m ²
B2_w-46 Nylon 2	172° (160° quick)	28.3 MPa	17 kN/m ²
B2_w-46 Nylon 3	170° (155° quick)	77.7 MPa	50 kN/m ²
B2_w-47 Nylon 1	170° (150° quick)	75.6 MPa	80 kN/m ²
B2_w-47 Nylon 2	165° (145° quick)	116.8 MPa	120kN/m ²

Tab. 5–5: Test and Analysis Results Nylon¹ Hinges

The test results confirm the expected correlation between a large Reopening-force and large von Mises stresses. But the correlation between Reopening-angle and Maximum von Mises Stress is smaller than expected.

On the one hand, the best Reopening-angles, 172° and 175°, also have a low Maximum von Mises Stress (44.6 MPa and 28.3 MPa), and the worst Reopening-angles, both 165°, have a large Maximum von Mises Stress (79.9 MPa and 116.8 MPa). On the other hand, the Maximum von Mises Stresses of 32.6 MPa and 151.3 MPa both lead to a Reopening-angle of 170°. While 44.6 MPa leads to a better, and 79.9 MPa leads to a worse Reopening-angle.

Possible reasons for this are:

- The printed Hinges are outside the validity range of the linear material model.
- The Tensile Modulus and Yield Stress were used instead of the Flexural Modulus, because no Flexural Yield Stress was provided. Furthermore, the material characteristics of small 3D printed Hinges may deviate from the general Nylon datasheet. For example, the alignment of layers have an influence in such small parts, while the material characteristics in the datasheet are isotropic.
- The Reopening-angle results are close to each other, especially when considering a deviation of a few degrees between each specimen of the same Hinge design. This may explain the irregular correlation between Reopening-angle and Maximum von Mises Stress.

5.3.3 2TR-Hinge

The 2TR-Hinge design requires very thin Torsion-Rods, which is too small for the Mark Two printer. However, one Hinge geometry could be printed with a “workaround”. A design with one thick Torsion-Rod without infill leads to a print of two thin Torsion-Rods. The test results are shown in Tab. 5–6.

Name	Test Results	Analysis Results	
	Reopening-angle	Maximum von Mises Stress	Reopening-force
2TR B2_w-45 Nylon 1	180° (160° quick)	35.9 MPa	70 kN/m ²

Tab. 5–6: Test and Analysis Results Nylon¹ 2TR-Hinges

The 2TR design is the best so far. The Reopening-angle reaches 180° within minutes. It also has a large Reopening-force, while the Maximum von Mises Stress is relatively low.

5.4 Conclusion

The correlation between von Mises stress and Reopening-angle is small. For a good prediction of the Reopening-angle and Reopening-speed, other material characteristics, like the “Elongation” and “Shore Hardness” might need to be taken into account.

Durable material takes too long to reopen and its parts are curved after printing. Therefore Nylon will be used for the Validation Test, even though the Mark Two printer requires thicker parts for printing precise Hinges.

Overall, the Nylon Hinge designs were improved. The tests in Chapter 4.3.2 showed Reopening-angles of 140° to 170°. After improving the design with a FEA (and being downgraded through automatic design changes by the printer), the Reopening-angles were between 165° and 180°.

¹ The Nylon yield stress is 31 MPa

These results are sufficient as a proof of concept for 3D-printed Hinges. Further optimization of the Torsion-Hinge design needs a set of requirements, regarding the materials and needed stiffness.

6 Summary and Outlook

6.1 Summary

To reduce the volume and mass of membrane deployment and stiffening for space applications, new methods were investigated. Every possible partial solution for the Deployment Method, Stiffening Structure, Distribution of Stiffening Structure and Packaging, was systematically structured in a morphological box. These partial solutions were combined to form whole concepts, which were evaluated.

The concepts regarded as most promising, use small rods in a specific pattern on the membrane. To avoid permanent deformation of the rod at the membrane folding lines, elastic hinges were developed and improved. These “Hinges” were identified as a critical component for many concepts and were therefore investigated in detail.

The main issues are the Reopening-angle and the stability of the Hinge. Rapid prototyping with 3D printing and hands-on testing of many different Hinge designs and materials led to a few promising designs and fitting material characteristics. These were evaluated and the Torsion-Hinge design was selected, together with the materials Nylon and Durable, for a Finite Element Analysis.

A parametric FE-model, that will be used as a basis in follow-up studies, was created and several improved Torsion-Hinge geometries were identified. These were printed, tested and had larger Reopening-angles than previously. The “B2_w-46 Nylon 1 Torsion-Hinge” had a Reopening-angle of 175° , while the “2TR B2_w-45 Nylon 1 Hinge” had one of 180° . This proves the applicability of a 3D printed elastic Hinge.

In order to validate the FEA by test data, a validation test should be conducted as the next step of the project, following this thesis.

6.2 Validation Test Preparations

An exemplary test setup and the necessary analysis changes to accommodate the test setup are presented here. However, FEA results are not presented, because the final test setup might be different, making the results obsolete.

The suggested test method is taken from [63] and its setup, the Counter-Weight Balanced Column Bending Test (CWB CBT) fixture, was developed by Opterus R&D and is shown in Fig. 6–1.

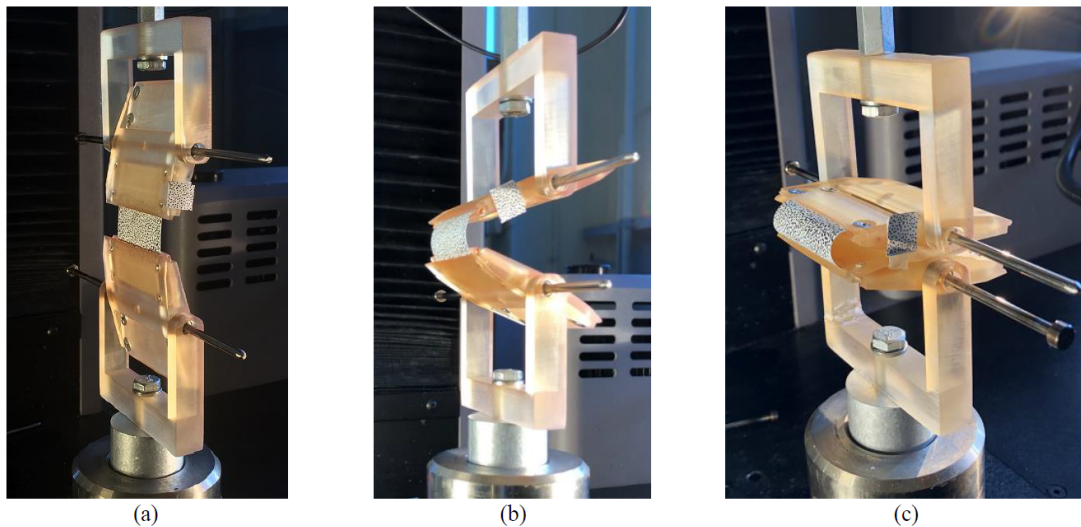


Fig. 6–1: Counter-Weight Balanced Column Bending Test Fixture at different stages of rotation [63]

Both rods of the Hinge are mounted in the fixture, with 5 mm distance¹ to the Torsion-Rod. In the middle of the 30 mm long fixture is a metal bar, parallel to the Torsion-Rod that connects the fixture to an actuator. The actuator pushes the rods together in a vertical lateral movement, as seen in Fig. 6–1 for a different specimen. The angle between the rods is computable from the position of the metal bars, or can be measured with a protractor.

In line with the actuator and fixture is a sensitive load cell, which is capable of measuring small "Displacement-forces". This force is parallel to the initial Hinge position, while the Reopening-force, which is more interesting regarding stability characteristics, is perpendicular to the rod. The smaller is the Displacement-angle the bigger the difference between Displacement-force and Reopening-force. However, this test is not about stability but for FEA validation. Therefore, the Displacement-angle is adequate.

These two values result in a force vs. angle graph.

The FEA has to be adapted to accommodate these changes to make testable predictions about what force leads to what angle.

The adaptations are:

The rod mounted in the fixture: The exact fixture and clamping do not have to be modelled. As simplification, a hard block of roughly the size seen in Fig. 6–1 can be connected to the 5 mm long Nylon rod, as if they are one part.

The transmission of force: The force and the boundary conditions are applied to metal bars in the middle of the fixture-blocks. The sliding properties between the fixture material and the metal bar have to be simulated by the friction coefficient.

The direction of gravity: +x Direction.

¹ No detailed size requirements are given, since the fixture/test setup has to be newly built at DLR.

Because the FE model is perfectly symmetrical, the Hinge is compressed instead of bent to one side. To make the Hinge in the FEA bend like the one in the test, a small initial displacement or force towards the bending direction might be needed.

The validation test can be done with the "B2_w-45 Nylon" Torsion Hinge (the printer software did not change its parameters) or a newly designed bigger Hinge, to decrease the effect of manufacturing imperfections (recommendation: minimum thickness 1.2 mm).

6.3 Outlook

The next step is to build the described test stand and conduct the validation test. If the test results do not match the FEA output, the FEA has to be adapted. The main possible changes to the FEA are the material characteristics and friction between the metal bar and the fixture.

When the FEA is validated, the parametrisation (described in Chapter 5) should take place. This will result in optimal geometries, depending on the desired output. (For example, the optimal Torsion-Hinge parameters for a 1 mm wide rod, where stability is more important than the Reopening-force.)

This parametrisation should be repeated for circular Hinges (O2-, Filled-O-, Oval-, Stretched-O-Hinge). For this, the geometry of the FE model has to be changed, so that an inner and outer, primary and secondary radii define the shape.

The results of both parametrisations should be compared to find the best Hinge design. However, this design, is dependent on the material characteristics. Therefore, if possible, the potential materials (and manufacturing method) for the parabola flight should be selected before performing the parametrisation. This parametrisation can include using different materials for different Hinge-parts, orientating on the results of Chapter 4.3.3. Otherwise, the best Hinge design for Nylon can be seen as the starting point for later parametrisation with a different material.

The effects of long term storage/folding have to be tested, as soon as the materials are selected.

The membrane has to be added to the FEA and tests with the right membrane and rod material have to confirm a successful reopening. Then, the distribution of rods on the membrane can be added to the FEA to start the superordinate development of the whole stiffened self-deploying membrane.

A slightly different and simpler approach to the overall solution of stiffened self-deploying membranes is to use the parametrisation to develop "Standard Hinge Elements". This means to find the optimal Hinge, for example, for 0.5 mm, 1 mm and 2 mm wide rods. Then, the distribution of rods and Hinges on the membrane can be done by sticking together rods and hinges with these three different thicknesses. This method



is an alternative to using elaborate simulations to find out the best placement and exact sizes of every rod and hinge.

Bibliography

- [1] W. K. Belvin, M. Straubel, J. Fernandez, M. E. Zander, M. Hillebrandt, and K. Wilkie, "Advanced deployable structural systems for small satellites," NASA & DLR, Ed., 2016.
- [2] "James webb space telescope: Goddard space flight center," NASA, Ed. [Online]. Available: <https://jwst.nasa.gov/facts.html#top> (Accessed 21.02.2018).
- [3] T. Sprowitz, P. Seefeldt, J. T. Grundmann, P. Spietz, N. Toth, M. Hillebrandt, M. Straubel, and M. E. Zander, "Design of the gossamer-1 deployment demonstrator," in *Proceedings of The Fourth International Symposium on Solar Sailing*, Japan Space Forum, Ed., 2017. [Online]. Available: https://elib.dlr.de/111055/1/17023_Paper_Mr.%20Tom%20Sproewitz.pdf
- [4] M. Straubel, M. Hillebrandt, and C. Hühne, "Evaluation of different architectural concepts for huge deployable solar arrays for electric propelled space crafts," DLR, Ed., 2016.
- [5] "Cubesat design specification rev. 13," California Polytechnic State University, Ed., 20.02.2014.
- [6] M. E. Zander, "Development of a structure supported membrane for deployable space applications," Diploma thesis, Otto von Guericke University, Magdeburg, 2010.
- [7] D. L. Chandler, "While you're up, print me a solar cell: New mit-developed materials make it possible to produce photovoltaic cells on paper or fabric, nearly as simply as printing a document." MIT News Office, Ed. [Online]. Available: <http://news.mit.edu/2011/printable-solar-cells-0711> (Accessed 09.02.2018). 11.07.2011.
- [8] D. L. Chandler, "Solar cells as light as a soap bubble: Ultrathin, flexible photovoltaic cells from mit research could find many new uses." MIT News Office, Ed. [Online]. Available: <http://news.mit.edu/2016/ultrathin-flexible-solar-cells-0226> (Accessed 09.02.2018). 25.02.2016.
- [9] "Best research-cell efficiencies," National Renewable Energy Laboratory, Ed. [Online]. Available: <https://www.nrel.gov/pv/assets/images/efficiency-chart.png> (Accessed 08.03.2018).
- [10] "Move-ii – munich orbital verification experiment ii," Technical University Munich, Ed. [Online]. Available: <https://www.move2space.de/MOVE-II/> (Accessed 05.03.2018).
- [11] MMA Design LLC, "Existing hawk configurations," MMA Design LLC, Ed. [Online]. Available: <https://mmadesignllc.com/products/solar-arrays/> (Accessed 16.09.2018).

- [12] “Re-entry: Flock 1b-6,” Spaceflight 101, Ed. [Online]. Available: <http://spaceflight101.com/re-entry/re-entry-flock-1b-6-2/> (Accessed 05.03.2018). 23.08.2016.
- [13] A. Kauderer, “Photo index 2,” NASA, Ed. [Online]. Available: <https://spaceflight.nasa.gov/gallery/images/shuttle/sts-116/html/iss014e10053.html> (Accessed 05.03.2018). 09.11.2012.
- [14] C. L. Foster, M. L. Tinker, G. S. Nurre, and W. A. Till, “Solar-array-induced disturbance of the hubble space telescope pointing system,” *Journal of Spacecraft and Rockets*, vol. 32, no. 4, pp. 634–644, 1995.
- [15] “Nasa - roll-out solar array (rosa),” NASA, Ed. [Online]. Available: https://www.nasa.gov/mission_pages/station/research/experiments/2139.html (Accessed 20.02.2018). 07.12.2017.
- [16] M. Killian, “Photos: Atk validates new megaflex solar array technology for nasa’s future solar electric propulsion missions,” Americaspace, Ed. [Online]. Available: <http://www.americaspace.com/2014/05/04/photos-atk-validates-new-megaflex-solar-array-technology-for-nasas-future-solar-electric-propulsion-missions/> (Accessed 14.02.2018).
- [17] “Ultraflex_factsheet,” Orbital ATK, Ed. [Online]. Available: https://www.orbitalatk.com/space-systems/space-components/solar-arrays/docs/UltraFlex_Factsheet.pdf (Accessed 14.02.2018).
- [18] “Solar sail,” Wikipedia, Ed. [Online]. Available: <https://en.wikipedia.org/w/index.php?oldid=828287841> (Accessed 06.03.2018). 03.03.2018.
- [19] R. Nemiroff and J. Bonnell, “Astronomy picture of the day: Nanosail-d,” R. Nemiroff and J. Bonnell, Eds. [Online]. Available: <https://apod.nasa.gov/apod/ap110128.html> (Accessed 06.03.2018). 28.01.2011.
- [20] Y. Miyazaki, “Deployable techniques for small satellites,” *Proceedings of the IEEE*, vol. 106, no. 3, pp. 471–483, 2018.
- [21] M. E. Zander, A. Wilken, M. Sinapius, and C. Hühne, “Mechanical testing of deployable thin shell cfrp booms in ideal and realistic interfaces for the solar sail demonstrator gossamer-1,” in *14th European Conference on Spacecraft Structures, Materials and Environmental Testing (ECSSMET)*, Insight Outside, Ed., 2016.
- [22] C. Sickinger and J. Melcher, “Entfaltungsmechanismen für den leichtbau auf basis bionischer elemente,” *DLR Interner Bericht*, p. 22, 2005.
- [23] “The james webb space telescope,” NASA, Ed. [Online]. Available: <https://jwst.nasa.gov/sunshield.html> (Accessed 07.03.2018).
- [24] J. A. Faber, A. F. Arrieta, and A. R. Studart, “Bioinspired spring origami,” *Science (New York)*, vol. 359, no. 6382, pp. 1386–1391, 2018.

- [25] F. Haas, S. Gorb, and R. Wootton, "Elastic joints in dermapteran hind wings: Materials and wing folding," *Arthropod Structure & Development*, vol. 29, no. 2, pp. 137–146, 2000. [Online]. Available: [https://doi.org/10.1016/S1467-8039\(00\)00025-6](https://doi.org/10.1016/S1467-8039(00)00025-6)
- [26] M. Mayser, "Entfaltungsmechanismen für den leichtbau auf der basis bionischer elemente," Diplomarbeit, Technischen Universität Braunschweig, Braunschweig, 20.04.2005.
- [27] S. A. Combes and T. L. Daniel, "Flexural stiffness in insect wings. i. scaling and the influence of wing venation," *The Journal of experimental biology*, vol. 206, no. Pt 17, pp. 2979–2987, 2003.
- [28] D. J. Tenenbaum, "Bats on the wing," T. Devit, Ed. [Online]. Available: <https://whyfiles.org/2014/bats-on-the-wing/index.html> (Accessed 13.03.2018). 21.07.2017.
- [29] "Leaf overview," University of Miami, Ed. [Online]. Available: <http://www.bio.miami.edu/dana/dox/leaf.html> (Accessed 12.03.2018). 05.04.2012.
- [30] "feuille verte isolée sur fond noir images photos gratuites," Fotomelia, Ed. [Online]. Available: <http://fotomelia.com/?download=feuille-verte-isolee-sur-fond-noir-images-photos-gratuites> (Accessed 12.03.2018).
- [31] H. Kobayashi, B. Kresling, and J. F. V. Vincent, "The geometry of unfolding tree leaves," *Proceedings of the Royal Society B: Biological Sciences*, vol. 265, no. 1391, pp. 147–154, 1998.
- [32] J. F. V. Vincent, "Chapter 2: Deployable structures in nature," in *Deployable structures*, ser. Courses and lectures / International Centre for Mechanical Sciences, S. Pellegrino, Ed. Wien: Springer, 2001.
- [33] S. Hobbs, J. Kingston, P. Roberts, C. Juanes, R. Sewell, B. Snapir, F. Robinson, J. Vigili Llop, J. Hobbs, and M. Patel, "De-orbit sail design for techdemosat-1," in *Proceedings of 6th European Conference on Space Debris*, ser. ESA SP, L. Ouwehand, Ed. Noordwijk: ESA Communications, 2013, vol. 723, p. 85.
- [34] A. Brinkmeyer, S. Pellegrino, and P. M. Weaver, "Effects of long-term stowage on the deployment of bistable tape springs," *Journal of Applied Mechanics*, vol. 83, no. 1, 2015.
- [35] Ö. Soykasap, "Analysis of tape spring hinges," *International Journal of Mechanical Sciences*, vol. 49, no. 7, pp. 853–860, 2007.
- [36] D. P. Cadogan and M. S. Grahne, "Deployment control mechanisms for inflatable space structures," in *33 rd Aerospace Mechanisms Conference*, NASA, Ed., 20.05.1999, (Accessed 07.03.2018).
- [37] "Cosmos 1," Wikipedia, Ed. [Online]. Available: <https://en.wikipedia.org/w/index.php?oldid=809300646> (Accessed 07.03.2018). 03.03.2018.

- [38] "Shape-memory alloy," Wikipedia, Ed. [Online]. Available: <https://en.wikipedia.org/w/index.php?oldid=828036284> (Accessed 14.03.2018). 28.02.2018.
- [39] L. R. Hill, G. Carman, D.-G. Lee, and B. Patrick, "Shape memory alloy film for deployment and control of membrane apertures," in *Optical Science and Technology, SPIE's 48th Annual Meeting*, ser. SPIE Proceedings, H. A. MacEwen, Ed. SPIE, 2003, p. 271.
- [40] "Electroactive polymers," Wikipedia, Ed. [Online]. Available: <https://en.wikipedia.org/w/index.php?oldid=833505327> (Accessed 09.04.2018). 03.04.2018.
- [41] T. Inamoria, Y. Satoub, Y. Sugawarac, and H. Ohsakia, "Electromagnetic panel deployment and retraction in satellite missions," *Acta Astronautica*, vol. 109, pp. 14–24, 2015. [Online]. Available: <http://dx.doi.org/10.1016/j.actaastro.2014.11.035> (Accessed 21.03.2018).
- [42] M. Arya, N. Lee, and S. Pellegrino, "Wrapping thick membranes with slipping folds," in *2nd AIAA Spacecraft Structures Conference 2015*. Red Hook, NY: Curran, 2015.
- [43] J. F. V. Vincent, "Chapter 4: How to fold a membrane," in *Deployable structures*, ser. Courses and lectures / International Centre for Mechanical Sciences, S. Pellegrino, Ed. Wien: Springer, 2001.
- [44] D. S. A. de Focatiis and S. D. Guest, "Deployable membranes designed from folding tree leaves," *Philosophical transactions. Series A, Mathematical, physical, and engineering sciences*, vol. 360, no. 1791, pp. 227–238, 2002.
- [45] H. Nakanishi, H. Sakamoto, H. Furuya, M. Yamazaki, Y. Miyazaki, A. Watanabe, K. Watanabe, A. Torisaka-Kayabe, and M. Oda, "Development of nano-satellite origamisat-1 with highly functional deployable membrane," in *Proceedings of The Fourth International Symposium on Solar Sailing*, Japan Space Forum, Ed., 2017, pp. 1–4. [Online]. Available: http://www.jsforum.or.jp/ISSS2017/papers/paper/17085_Paper_Prof.%20Hiroki%20Nakanishi.pdf (Accessed 07.05.2018).
- [46] M. Arya, N. Lee, and S. Pellegrino, "Ultralight structures for space solar power satellites," in *3rd AIAA Spacecraft Structures Conference*. Reston, Virginia: American Institute of Aeronautics and Astronautics, 2016.
- [47] "Pvc-dach / profiliert," Archiexpo, Ed. [Online]. Available: <http://www.archiexpo.de/prod/ondumit/product-155986-1842641.html> (Accessed 21.03.2018).
- [48] "Amazon.in: Themisto 12volt dc motor," Amazon, Ed. [Online]. Available: <https://www.amazon.in/Themisto-12Volt-Multipurpose-Brushed-applications/dp/B06XC6XY7R> (Accessed 21.03.2018).
- [49] "Faltbare frisbee," VH-Werbeartikel, Ed. [Online]. Available: <http://www.vh-werbeartikel.de/werbeartikel/faltbare-frisbee-3710> (Accessed 21.03.2018).

- [50] "Excel assemblies: Cable harness," Excel Assemblies, Ed. [Online]. Available: <https://www.excel-assemblies.com/de/kompetenzen-produkte/> (Accessed 21.03.2018).
- [51] N. Heinz, "Elektrospulen - homofaciens," Homofaciens, Ed. [Online]. Available: https://www.homofaciens.de/technics-electrical-engineering-inductor_ge.htm (Accessed 21.03.2018). 2009.
- [52] M. Kretzer, "Electroactive polymers: polymers that can change their shape in response to a strong electrical field," Materiability, Ed. [Online]. Available: <http://materiability.com/portfolio/electroactive-polymers/> (Accessed 09.04.2018). 2013.
- [53] "The all-new makerbot replicator+," MakerBot Industries, Ed. [Online]. Available: <https://www.makerbot.com/3d-printers/replicator/> (Accessed 21.06.2018).
- [54] "Original prusa i3 mk2s 3d drucker bausatz," Prusa Research s.r.o, Ed. [Online]. Available: <https://www.prusa3d.de/kit-de/> (Accessed 21.06.2018). 21.06.2018.
- [55] "Form 2 desktop sla 3d-drucker produktinformationen," I. Formlabs, Ed. [Online]. Available: <https://formlabs.com/de/3d-printers/form-2/> (Accessed 21.06.2018).
- [56] "Der mark two 3d-drucker von markforged," Mark3D GmbH, Ed. [Online]. Available: <https://www.mark3d.com/de/markforged-mark-two/> (Accessed 21.06.2018).
- [57] "Connex3 objet260," Stratasys Ltd., Ed. [Online]. Available: <http://www.stratasys.com/3d-printers/objet260-connex3> (Accessed 21.06.2018).
- [58] "Flexible: Photopolymer resin for form 1+ and form 2," I. Formlabs, Ed. [Online]. Available: <https://formlabs.com/media/upload/Flexible-DataSheet.pdf>
- [59] "Durable: Photopolymer resin for form 2," I. Formlabs, Ed. [Online]. Available: <https://formlabs.com/media/upload/Durable-DataSheet.pdf>
- [60] "Materialspezifikationen verbundwerkstoffe," Markforged, Ed. [Online]. Available: <https://www.mark3d.com/en/wp-content/uploads/sites/6/2018/03/Markforged-Composites-Datasheet.pdf> (Accessed 26.06.2018).
- [61] "Digital materials data sheet," Stratasys Ltd., Ed. [Online]. Available: www.stratasys.com/-/media/files/material-spec-sheets/mss_pj_digitalmaterialsdatasheet_0617a.pdf (Accessed 26.06.2018).
- [62] "Polyjet materials data sheet," Stratasys Ltd., Ed. [Online]. Available: http://global72.stratasys.com/~/-/media/Main/Files/Material_Spec_Sheets/MSS_PJ_PJMaterialsDataSheet_0517aWeb.pdf (Accessed 26.06.2018).
- [63] J. M. Fernandez and T. W. Murphey, "A simple test method for large deformation bending of thin high strain composite flexures," in *AIAA Spacecraft Structures Conference 2018*. Red Hook, NY: Curran Associates Inc, 2018.

A Appendix

A.1 Torsion Hinge Mesh

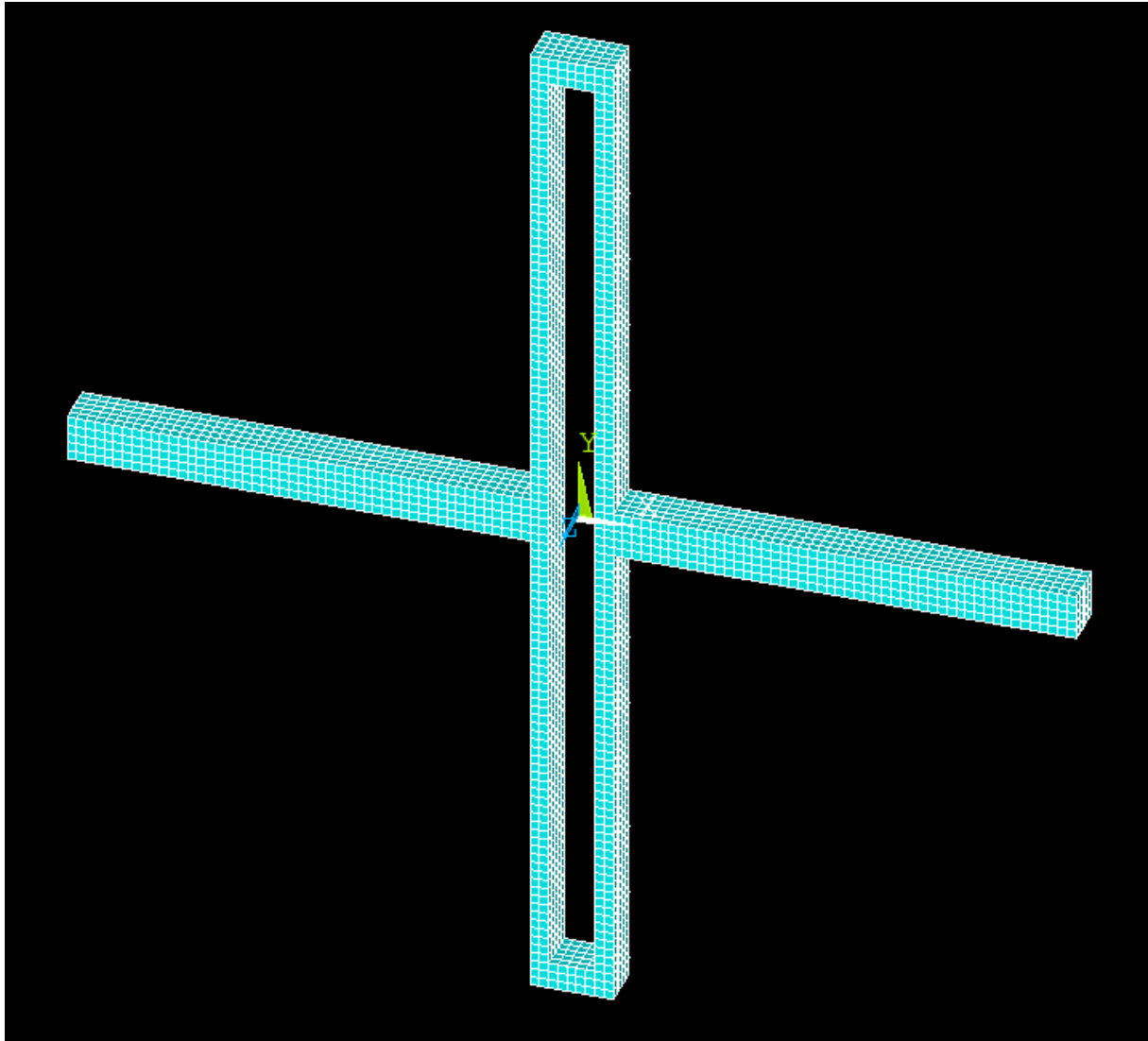


Fig. A.1: Mesh of the B2_w45 Nylon Hinge

A.2 Hinge Parameters

Name:		B2_w-37	B2_w-40	B2_w-40	B2_w-46	B2_w-46	B2_w-46	B2_w-47	B2_w-47
Parameter	Unit	Durable	Nylon 1	Nylon 2	Nylon 1	Nylon 2	Nylon 3	Nylon 1	Nylon 2
B1_h	mm	1	2	2	2	2	2	2	2
B1_l	mm	15	20	20	20	20	20	20	20
B1_w	mm	1	2	2	2	2	2	2	2
B2_h	mm	1	1.5	1.5	1.5	1.5	1.5	2	2
B2_l wanted	mm	0.7	0.6	0.8	0.7	0.7	0.8	0.7	0.8
B2_l printed ¹	mm		1.8	1.2	1.2	0.7	1.2	1.2	1.6
B2_w	mm	37	40	40	46	46	46	47	47
B3_h	mm	1	1.5	1.5	1.5	1.5	1.5	2	2
B3_l	mm	1	1	1	1	1	1	1	1
B3_w wanted	mm	0.8	0.8	0.8	0.6	0.6	0.8	0.8	0.8
B3_w printed ¹	mm				2	1			
Mat_Density	kg/m ³	1000	1100	1100	1100	1100	1100	1100	1100
Mat_Young's modulus	MPa	820	940	940	940	940	940	940	940
Mat_Poisson's ratio		0.39	0.4	0.4	0.4	0.4	0.4	0.4	0.4
Mat_Yield stress	MPa	27.2	31	31	31	31	31	31	31
Mesh Size	m	0.0004	0.0004	0.0004	0.0004	0.0005	0.0004	0.0005	0.0004
Reopening-force	kN/m ²	30	100	55	55	17	50	80	120
Displacement-angle	°	167	182.6	175.2	181.4	181.9	186.1	180	173
Maximum von-Mises Stress	MPa	27.2	151.3	79.9	44.6	28.3	77.7	75.6	116.8

Tab. A.1: Parameters and Analysis Results of Torsion-Hinges

¹ These parameters were changed by the 3D printer (no change, if the field is empty). The analysis was repeated with these printed parameters.

A.3 Folded Bowl Hinge

The Bowl Hinges flexible part is made of a mixture of TangoBlack+ and RGD525.

Upper left picture: The walls ripped and are spreading to the sides.

Upper right picture: Folding completed.

Lower three pictures: Reopening of the Bowl Hinge lying on a piece of paper.



Fig. A.2: Folding and Reopening of the Bowl Hinge

A.4 Folded O-Hinge

The O-Hinge is made of Nylon in the Mark Two printer. You can see manufacturing imperfections in the O-part, caused by a unprecise printer or a too small Hinge.



Fig. A.3: Folding of the O-Hinge